

ON THE VIBRATORY RESPONSE OF THE
STANDALONE ATOMIC FORCE
MICROSCOPE

By

THOMAS MARELLI

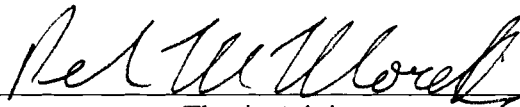
Bachelor of Science
The University of Oklahoma
Norman, Oklahoma
1991

Bachelor of Arts
The University of Oklahoma
Norman, Oklahoma
1991

Submitted to the Faculty of the
Graduate College of the
Oklahoma State University
in partial fulfillment of
the requirements for the Degree of
MASTER OF SCIENCE
May, 1995

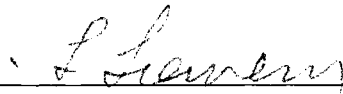
ON THE VIBRATORY RESPONSE OF THE
STANDALONE ATOMIC FORCE
MICROSCOPE

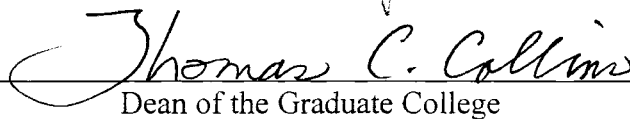
Thesis Approved:



Thesis Adviser

Don A. Luman





Dean of the Graduate College

ACKNOWLEDGEMENTS

In acknowledgement of Professors Moretti, Lucca and Lowery, who provided the essence of my education at Oklahoma State University. Their instruction brought me on the cutting edge of technology, while their guidance launched me into a promising career. My appreciation also goes to Dr. Price who gave me the opportunity to enter the graduate program. Special Thanks to Dr. Leider Professor and Director of Landscape Architecture through whom I learned ethics and diplomacy.

I hope that in the future I can represent Oklahoma State University with distinction.

TABLE OF CONTENTS

Chapter	Page
I. INTRODUCTION	1
Overview	1
Hardware Description.....	2
Software Description	3
II. LITERATURE REVIEW.....	6
Summary	7
III. PRELIMINARY ASSESSMENTS	8
Vibrations Effects on Output.....	8
Feedback Response	8
Upper Bounds for Vibration Detection	9
Spatial Vs. Temporal Disturbances	11
Summary	12
IV. EXPERIMENTATION.....	14
Data Acquisition and Equipment	14
V. RESULTS	16
Equipment Calibration	16
Room Resonances	17
Scanning Parameters	18
Piezoelectric Motor Speed.....	19
Free Response Test.....	19
Thermal Effects	21
Conclusion.....	22
VI. MODELING	23
One Dimension.....	23
Two Dimensions.....	25

VII. DISCUSSION	33
Vibration Isolation.....	33
Conclusions	34
BIBLIOGRAPHY	37
APPENDIXES	38
APPENDIX A-AFM MODEL	39
APPENDIX B-SIMULATION PROGRAM.....	42
APPENDIX C-ISOLATION DESIGNS	45
APPENDIX D-VIBRATION DATA	49

LIST OF TABLES

Table	Page
d.t.1. Resonances.....	52
d.t.2. Vibrations and Scanning Parameters Relations.....	53
d.t.3. Piezo Speed Limit.....	54
d.t.4. Free Response on Hard Disk.....	67
d.t.5. Free Response on Glass.....	75
d.t.6. Free Response on Isolation Platform.....	81

LIST OF FIGURES

Figure	Page
1. StandAlone Atomic Force Microscope.....	4
2. Deflection and Compensation.....	10
3. Temporal and Spatial Relations.....	13
4. Support Rig.....	20
5. One Dimensional Dynamic Absorber.....	23
6. Simulation Set-up.....	25
7. Simulation of One Dimensional Model.....	25
8. Two Dimensional Dynamic Absorber.....	26
9. Simulation of a Two Dimensional Model.....	28
10. Simulation of a Two Dimensional Model.....	29
11. Simulation of a Two Dimensional Model.....	30
12. Simulation of a Two Dimensional Model.....	31
13. Simulation of a Two Dimensional Model.....	31
14. Three Dimensional Atomic Force Microscope Scans.....	36
a.1. StandAlone Microscope Model.....	39
c.1. Conceptual Rig Design for Inverted Scanning.....	46
c.2. Conceptual Design for Inverted Scanning of Computer Hard Disks.....	47
c.3. Combined Isolation Devices.....	48

d.1. Vibrations and Scanning Speed	50
d.2. Surface Features.....	51
d.3. Scan # 1.021.....	55
d.4. Scan # 1.022.....	56
d.5. Scan # 1.023.....	57
d.6. Scan # 1.024.....	58
d.7. Scan # 1.025.....	59
d.8. Scan # 1.027.....	60
d.9. Scan # 1.028.....	61
d.10. Scan # 2.000.....	62
d.11. Scan # 2.001.....	63
d.12. Scan # 2.002.....	64
d.13. Scan # 2.003.....	65
d.14. Scan # 2.004.....	66
d.15. Scan # 1.031.....	68
d.16. Scan # 1.031.....	69
d.17. Scan # 1.033.....	70
d.18. Scan # 1.033.....	71
d.19. Scan # 1.034.....	72
d.20. Scan # 1.035.....	73
d.21. Scan # 1.036.....	74
d.22. Scan # 1.036.....	76
d.23. Scan # 2.010.....	77

d.24. Scan # 2.012.....	78
d.25. Scan # 2.017.....	79
d.26. Scan # 2.017.....	80
d.27. Scan # 2.006.....	82
d.28. Scan # 2.008.....	83
d.29. Thermal Drifts.....	84

CHAPTER I

INTRODUCTION

Overview

Historically the demand to eliminate vibrations has extended to ever higher frequencies and ever lower amplitudes. In some cases process control is now in the nanometric range and acceptable errors are on an even smaller scale.

For surface analysis, the Scanning Electron Microscope gives very high resolution; but for practical purposes, deriving surface topography from scattering angles requires a lot of human interpretation. In the early 1980's the Scanning Tunneling Microscope was developed from the principle of ionizing the space between the sample and the microscope tip; the resulting tunneling current is a function of the distance between microscope tip and surface feature. Unfortunately this microscope can only be used with conductive sample. In 1985 G. Binnig, C. Gerber and C. Quate invented the Atomic Force Microscope. Within a certain proximity interatomic forces are a strong function of distance. A cantilever with a tip can bend around surface features without displacing atoms. Measured cantilever deflections can then be related to roughness.

The Atomic Force Microscope is a sensitive profilometer used for the measurement of surface features. In particular the StandAlone AFM is portable and it can be placed directly on the specimen. Just like any ultraprecision instrument it is greatly

influenced by ambient conditions. Imperfections in equipment construction and lack of knowledge of exact value of physical parameters impose limitations on the accuracy of AFM measurements. But of even greater interest is the repeatability of an experiment. Precision is affected in the long term by equipment degradation and replacement with different parts. In the short term, thermal drifts, air composition, vibration, and electromagnetic interference can cause errors during the scan of a sample. The most prominent of these factors appears to be that of vibrations.

One cannot hope to reproduce an experiment two separate times because the StandAlone cannot be repositioned exactly. Therefore repeatability of this study is limited to statistical properties. The following outline gives the scope of this study:

- i) Determine sources of vibrations.
 - a. Transmission through the ground.
 - b. Acoustic vibrations.
 - c. Vibrations generated by the system itself.
- ii) Measure vibrations.
- iii) Describe how various parts of the microscope are affected by vibrations.
- iv) Eliminate unwanted vibrations.

Hardware Description

The surface topography of a sample is resolved on a CRT by scanning with a sharp-tipped probe. A stack of piezoelectric material in the shape of a hollow cylinder provides the motion that guides the tip over the sample surface. The cantilever probe bends as its tip follows the surface profile, and the deflection is measured by way of laser

interferometer in the gap between the laser diode and the back of the cantilever. When the cantilever bends over some surface feature, the gap changes and causes variations in the intensity of the output beam. Changes in the output beam are detected by a photodiode and interpreted as height readings. There are two modes of operation from which surface topography is constructed. One mode uses voltage readings from the photodiode. Since the photodiode cannot discern between successive maxima, this mode is ideal for flat samples where the cantilever deflection is less than one half of the laser wavelength.

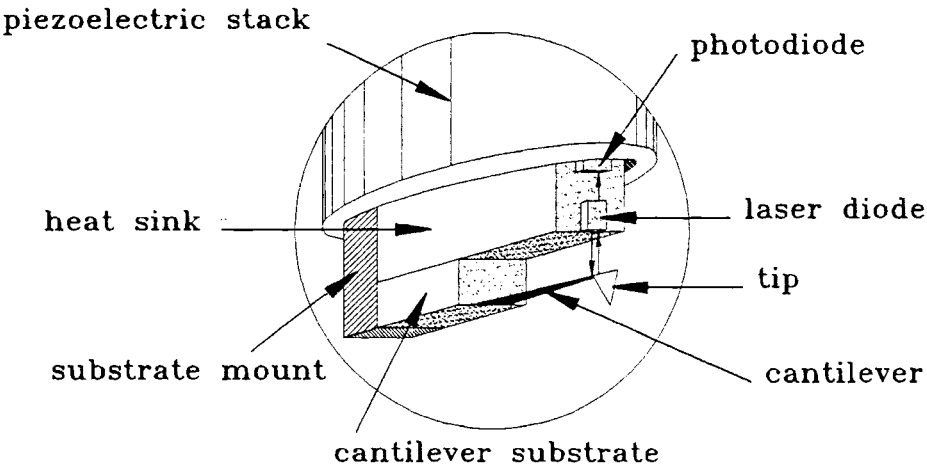
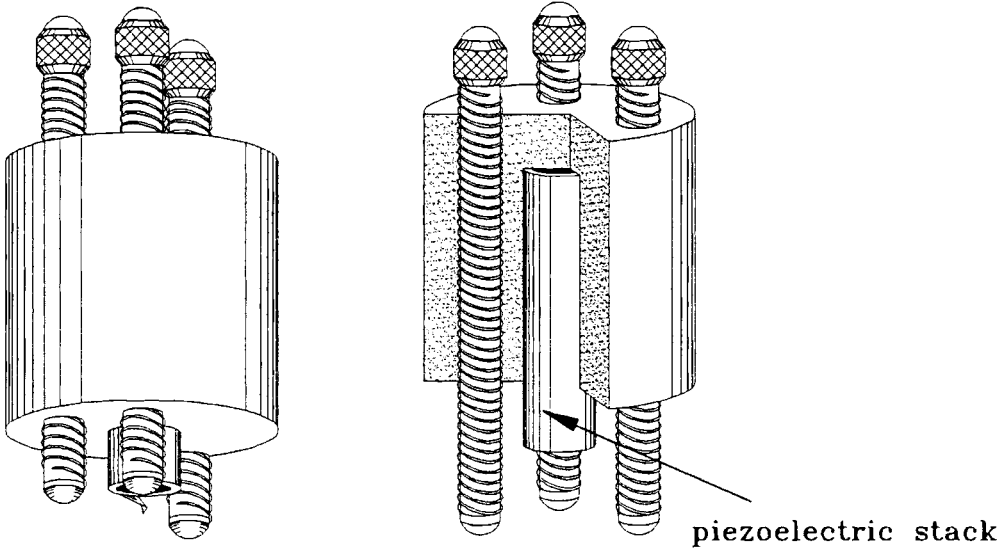
The alternate mode of operation makes use of feedback control to adjust the height of the piezo tube and maintain cantilever deflection constant. Extending and contracting of the piezo tube corresponds to changes in height of the surface profile. The voltage required to change the height of the piezo stack is used for creating the surface topography.

The system is encased in a metal shell that has three height adjustment screws running through it, as shown in figure 1.

Software Description

Vibrations can be observed in real time on the monitor display of the photodiode signal. Before the tip comes in contact with the surface the photodiode signal is a straight line, signaling constant output intensity from the laser cavity. As the tip comes in contact with the surface, the cantilever bends and the laser cavity begins to shorten.

Correspondingly the output intensity begins to vary sinusoidally and the display shows these changes. For example, a certain applied force might produce a cantilever deflection



Detail

Figure 1. StandAlone Atomic Force Microscope.

of two laser wavelengths, then a two cycle sinusoid appears on the display screen. The signal display is of interest because the sinusoid jumps showing clearly the presence of vibrations.

Piezo tube extension and retraction are governed by a feedback loop that may be adjusted to optimize the gains. When the integral and proportional gains are too high the piezo oscillates, producing high frequency waves in the scan. This indicates the maximum attainable speed by the piezo tube. Later it will be shown that this effect determines the higher bounds for vibration detection.

The software also features Fast Fourier Transform capabilities and power spectral density.

A preliminary observation indicates three places in the AFM where the vibrations may develop: in the height adjustment screws, in the cantilever assembly and in the motion induced in the piezo stack. These observations are the basis for some of the experiments presented in chapter III.

CHAPTER II

LITERATURE REVIEW

In 1993 there were about two hundred scientific publications on the Atomic Force Microscope, none of which dealt with vibrations. There are, however many studies done on other high resolution microscopes and sensitive equipment. Rivin (1979) investigates vibration isolation of precision machinery in a manner that relates to precision engineering.

In his book on measurement, Buzdugan (1986) gives a comprehensive listing of measuring equipment, its use and characteristics. This book is particularly useful in determining which equipment could measure at an atomic length without causing electromagnetic, mechanical or thermal interference.

Macinante (1984) wrote a book on isolation which is a purely qualitative analysis of various vibration studies. Even though the studies are for larger non-sensitive equipment, the book is useful for developing a systematic approach for design of an isolation system.

In his book Vibration, Inman (1989) gives a full exposition of the modern concepts of vibration studies. Topics like model reduction, damping design, model testing and analysis are tied in with principles of dynamic control. The range of topics is too broad to cover each in depth, nonetheless the book is ideal for designing a research

with cutting edge methodology.

Tiersen (1969) writes on the vibrations of piezoelectric plates. These studies provide theoretical means for calculating the limits of response of the piezo motor of the AFM. It will be shown later that this gives a bound for our ability to detect vibrations if the AFM itself is used for detection.

Summary

Collectively, the books listed above, are useful for establishing the general guidelines of the research project in question. Macinante gives some standard methods for designing an experiment, followed by some real studies. The text Vibration by Inman gives a very comprehensive listing of modern methods for measurement and analysis. And Buzdugan provides detailed technical information of measuring equipment.

The research can then be roughly charted from the topics of these books

1. Knowledge of microscope vibrations.
2. Experiment design.
3. Methods for measurements.
4. Measuring equipment.
5. Data analysis.

The next chapter presents some of the speculations made from studies prior to experimentation.

CHAPTER III

PRELIMINARY ASSESSMENTS

Vibrations Effects on Output

Some of the surface scans made prior to this study revealed some features that may not have been part of the samples. These observations combined with non repeatability of experiments led to the conclusion that the microscope may be affected by vibrations. In the real time display of a scan, an acoustic wave can be observed to cause a jump in the image tracing. This effect suggests the use of the microscope itself as a vibration detector, provided that its limitations are understood.

The chapter investigates the following features of AFM behavior:

- i) Interaction between feedback response and vibrations.
- ii) Limitations on vibration detection.
- iii) Ability to discern disturbances in time from spatial features.

Feedback Response

From the manual's description of the AFM configuration it appears that vibrations could be induced in the photodiode or in the laser diode. If the vibrations occur in the laser diode, the vibratory component parallel to the laser beam changes the resonator length and consequently the efficiency. This affects the output beam intensity, it triggers

the feedback loop to compensate, and it registers as a surface feature. Likewise, if the StandAlone or the test sample are undergoing vertical vibratory motion, the effect is the same as with the laser diode.

Three possible sources of vibrations that produce the same effect; this warrants a closer look at the situation. When the cantilever begins to deflect, the feedback loop begins to change the height of the piezo stack to keep the deflection constant. This way the laser oscillations never go through one half cycle of phase change inside the resonator. Suppose that the scan rate is high and the sample not very flat, this causes the cantilever to deflect faster than the feedback can compensate. Then, while the cantilever is still deflecting in one direction, the phase changes and the feedback loop 'thinks' that the deflection reverses. Compensation, then, begins in the wrong direction and the cantilever deflects even faster causing possibly another phase change. The resulting readings cannot be attributed to surface features. The AFM manual calls this effect fringe hopping. The above situation, also shown in fig. 2, is a key to understanding the vibration behavior of the AFM.

Upper Bounds for Vibration Detection

The analog to digital converter operates at 62.5 KHz, giving a sample period of 16 μ s. Each scan produces a square matrix of datapoints of dimensions $N \times N$. Each datapoint is an average of all the analog to digital conversions that occurred since the preceding datapoint.

The AD converter establishes immediately an upper bound to the frequencies that can be detected. The Nyquist criterion of sampling requires that the highest frequency

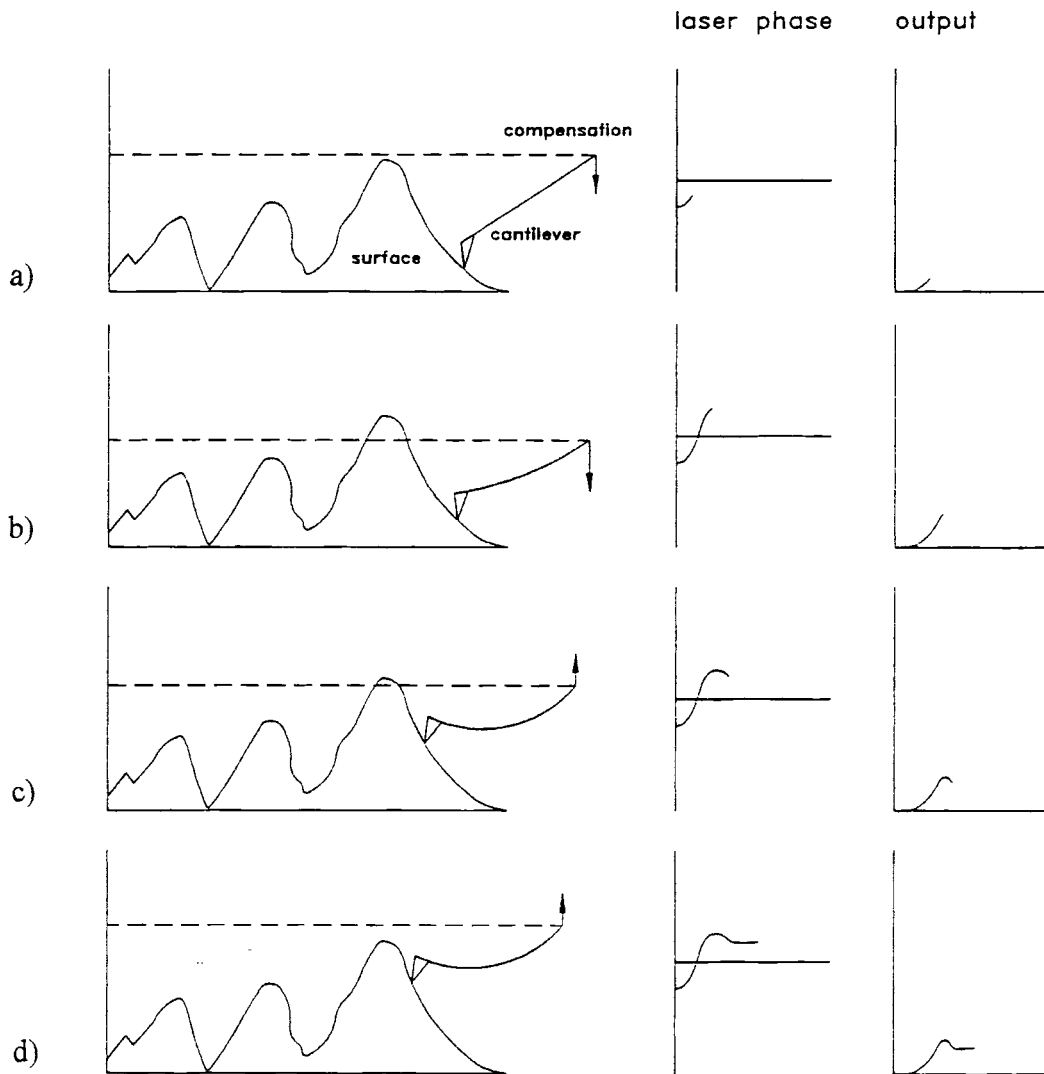


Figure 2. Deflection and compensation

- a) Cantilever begins to deflect and compensation engages
- b) Deflection exceeds compensation, laser phase begins to change
- c) Laser phase has changed by half cycle, compensation reverses
- d) Compensation is in the same direction as deflection, contour readings are incorrect

component is sampled twice per cycle, thus:

$$f_{\max} = 1/2 * \text{sampling rate}$$

Better results are obtained when the nominal bandwidth f_{\max} is sampled 2.5 times per cycle. Higher frequency spectral components that do not meet the Nyquist criterion are aliased down to lower frequencies, that is, they appear as lower frequency harmonics.

In the case of a 62.5 KHz AD converter:

$$f_{\max} = \frac{62.5 \text{ KHz}}{2.5} = 25.0 \text{ KHz}$$

However, since the sampling is averaged between datapoints, the nominal bandwidth depends on the frequency of datapoints. Additional limitations are imposed by the mechanical response of the piezo stack. Since the piezo motor can extend and retract at a certain maximum velocity, it can only follow surface features up to a certain frequency. Since feedback can provide compensation for any piezo speed, it does not impose limitations on f_{\max} . Therefore the cutoff where frequency spectral components begin to be aliased depends on the piezo motor and the frequency of datapoints. These concepts are crucial for a qualitative analysis of the vibration response of the AFM.

Spatial Vs. Temporal Disturbances

Vibrations of the equipment or the specimen are disturbances in time, while surface features are disturbances in space. When comparing cross sections of a scan made at different speeds the surface features appear the same, while vibrations appear at different wavelengths. Scanning at a higher speed would stretch out the wavelength of a vibration, then for the same number of datapoints f_{\max} would be higher, but the number of

samples would be less (figure 3a). Since both, piezo oscillations and vibration disturbances occur in time, increasing the scan speed does not increase f_{\max} (figure 3b). In conclusion the highest frequency disturbance that can be resolved is the same as the maximum piezo frequency, provided that there are at least 2.5 datapoints per cycle. Then for analytical purposes a free response test should have a smooth surface, few datapoints, high speed, and large scanning length; this way surface features would become invisible. The scanning speed should not be so high as to stretch the free response beyond the scanning length. Ideally the given impulse should not be so high as to produce frequencies greater than f_{\max} . The value of f_{\max} can be obtained by raising the gains to the point where the piezo begins to vibrate erratically. This point is the maximum attainable piezo speed.

Summary

By comparing scans of the same specimen made at different speeds, it is possible to sort out contours in space and in time. Although not all frequencies can be detected, the upper bounds for detections are known from the piezo motor speed. The mechanical constraints of the StandAlone are well documented, for this reason the AFM can become an effective tool for detecting vibrations.

The next chapter outlines procedures and equipment that will be used to set up artificial test conditions for conducting controlled experiments.

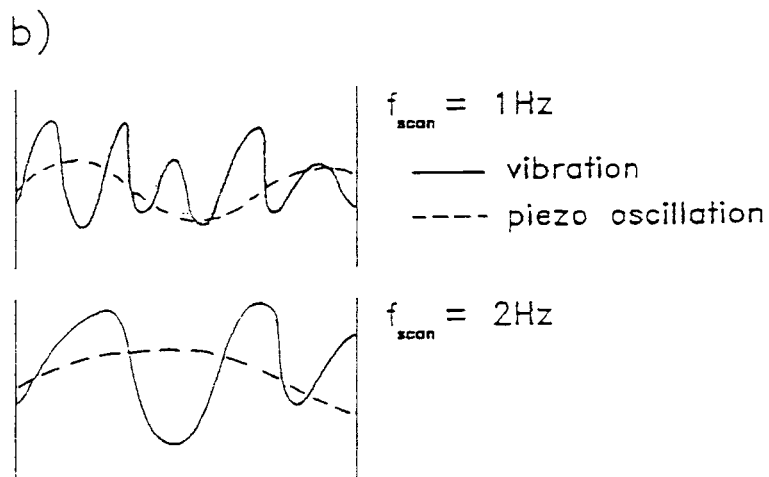
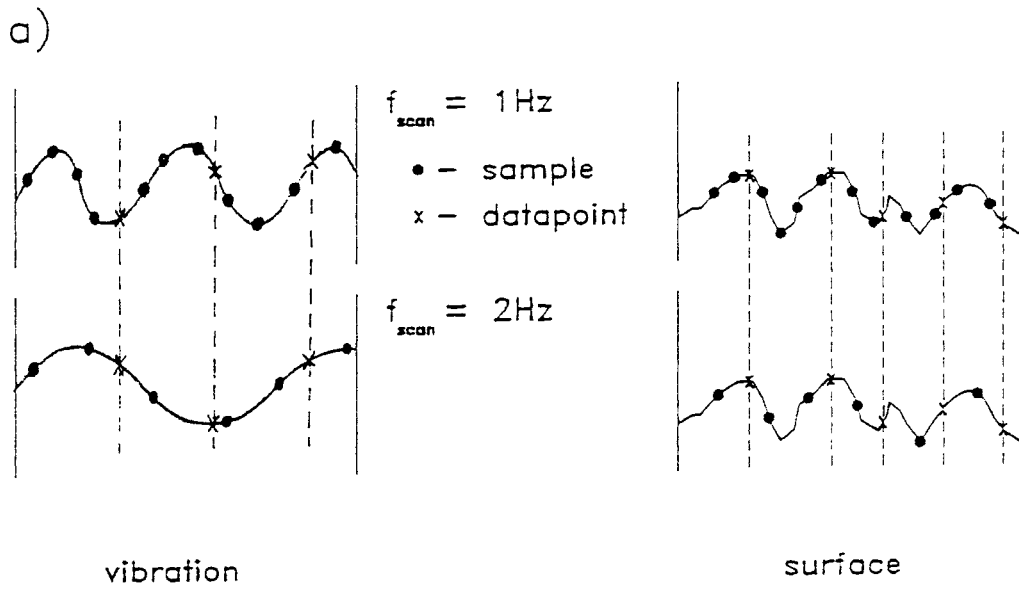


Figure 3. Temporal and spatial relations

CHAPTER IV

EXPERIMENTATION

Data Acquisition and Equipment

The crux of this study is to identify the resonant frequencies of the AFM for the purpose of designing some system for vibration control. Two methods are used for obtaining the natural frequencies: real time test of the response under a disturbance of varying frequency and the free response from an impulse. The two results can then be compared for discrepancies. The test procedure is outlined as follows:

- i) Room resonances are measured by identifying standing waves with a sound level meter.
- ii) A loudspeaker sweeps through a range of frequencies and microscope resonances are identified in the scan image.
- iii) The effects of various scanning settings (scan rate, gains, etc.) are observed by applying a known disturbance and varying the parameters of interest..
- iv) The free response from an impulse input is observed in cross sections of the scanned image.

The AFM itself is used to measure vibrations. Its software features a real time display of the image scanned, Fast Fourier Transform capabilities and power spectral density.

The generator for acoustic waves, HP Model 200 AB Audio Oscillator, is calibrated by the digital counter HP 5315B Universal Counter. All acoustic output is produced by a Realistic speaker with a 3 inch and a 2 inch cone in a vertical arrangement. Sound amplitude is measured by a sound level meter of the type Brüel & Kjaer 2203 with an octave filter set 1613.

The microscope and some other optical equipment rest on a large isolation table placed next to a desk with a computer. The room is approximately 15x7 feet and has an air diffuser on the ceiling. The floor is carpeted and the door has a wide gap at the bottom. The room is in a laboratory with various machines and other sources of systematic noise.

Testing procedures are initially devised without prior knowledge of subsequent difficulties that may be encountered. Consequently, the above guidelines are somewhat generalized. The next chapter presents a more detailed description of the experimental process, along with the results and new observations that arise during the procedures.

CHAPTER V

RESULTS

Equipment Calibration

All acoustic input is produced by a speaker with two cones of different sizes, in a vertical arrangement. The accuracy of the wave generator output is measured with a digital counter. In order to determine the relation between the input frequency and the frequency from the FFT diagram a known disturbance is applied. The FFT diagram produced a peak at the same frequency. Experiments are conducted at night to avoid noise from the activity of lab personnel. For control purposes all samples were first scanned without applied disturbances.

Temporal disturbances stretched out as predicted at higher scanning speeds, while spatial disturbances appeared the same. This effect can be seen in figure d.1 in the data section. Therefore with the knowledge of scanning speed wavelength and frequency, the viewer can determine whether a disturbance is a vibration or a surface asperity. This is perhaps the most powerful feature of the microscope for detecting vibrations. To test the conjecture that surface features become less visible at higher speeds and fewer datapoints, several scans were made from the same sample of a computer hard disk. The results shown in figure d.2. were concurrent with the above assumption. For a different specimen one might have to experiment with scan speed scan size, gains and other

parameters.

Room Resonances

Room resonances were measured by placing a sound level meter at the location of the microscope. Standing waves with the largest amplitudes were measured to be between 150 and 270 Hz.

To get a comprehensive idea of the interaction of room resonances with the vibrations excited in the AFM, the following experiments were made. A speaker was placed near the microscope and the microscope was replaced with a sound level meter. Sound was swept through a range of frequencies and the resonances were recorded. With the sound level meter in the same place, the speaker was moved to a corner of the room. As expected the speaker in the corner excited more resonances. The interesting result is that the frequencies found with the speaker in different locations are not all the same. This means that the modes excited in the room depend largely on the location of the source. A variety of parameters do not allow an exact evaluation of room modes or their interaction with the AFM. The room is small and when large equipment is moved or when personnel moves, the configuration of modes changes. The speaker itself has resonances. The observable response of the microscope has a frequency limited by the speed of the piezo motor.

The greatest responses of the AFM under excitation from the speaker are found in a bandwidth that coincides roughly with the room resonances of largest amplitude (table d.1.1.).

A partial solution to steady acoustic disturbances would be to simply move the

microscope to that location of the room which has a node at the frequency of greatest disturbance.

Scanning Parameters

In this set of experiments, vibrations are observed for a variety of scanning parameters. The first scan is for control purposes and contains no disturbances. A low value of acoustic amplitude necessary for a response is determined. The input frequencies are swept from 1 Hz to 20 KHz over three scans. Visible responses appeared at about 70 Hz and ended around 400 Hz. Three major resonances are identified and reproduced in the following experimental configurations.

- i) different scan rates
- ii) different number of samples
- iii) different gains
- iv) different applied cantilever force
- v) different scan sizes
- vi) scan in deflection mode

By looking at many cross sections, high amplitude responses were identified roughly at 215 Hz, 269 Hz and 279 Hz. These frequencies were fine tuned with the real time display of the photodiode signal. Where the sinusoid jumps the most, the AFM response is greatest. Resonances, were determined to be at 212.2 Hz, 267.4 Hz and 272 Hz. None of the responses showed any appreciable effect when the above parameters were changed (table d.t.2, figures d.3 - d.9).

Piezoelectric Motor Speed

One method of observing the limit for piezo speed is by increasing the gains until erratic oscillations are seen in the real time image of a scan. This measurement can be quantified with some degree of precision by scanning a sample at 1 Hz and finding an approximate frequency of the surface from the FFT. Scanning speed is then increased until the piezo can no longer reproduce the surface features. That is the limit for piezo speed and is given by: $f_{\text{piezo}} = f_{\text{sample}} * f_{\text{scan}}$. Table d.t.3 gives the scan numbers with respective incremental parameter changes. The resulting outputs are shown in Figures d.10 through d.14, where the tall feature to the right was used as a reference point.

Free Response Test

In order to circumvent the problem of interference from room and speaker modes, natural frequencies are derived from the response of the AFM. The first experiment consists of tapping lightly the microscope at different points. Scanning parameters were set as predetermined in the section Temporal Vs. Spatial Disturbances. The parameters for each scan are given in table d.t.4, and the results are shown in Figures d.15 through d.22. The results are most enlightening, all responses of the AFM mounted on the support rig (Figure 4) gave a peak at ~ 147 Hz, except for the 10 nm scan. Figure d.20 shows clearly that the readings for the 10 nm scan are not reliable due to the surface resolution. It was observed that tapping on the AFM leg induced a greater response. This suggests that the vibrations may not be in the laser diode, but rather, in the legs. When the AFM is scanning on the rig the legs are extended and the frequency of vibrations should be lower. Figures d.21 and d.22 show, as expected, a response at ~ 85 Hz.

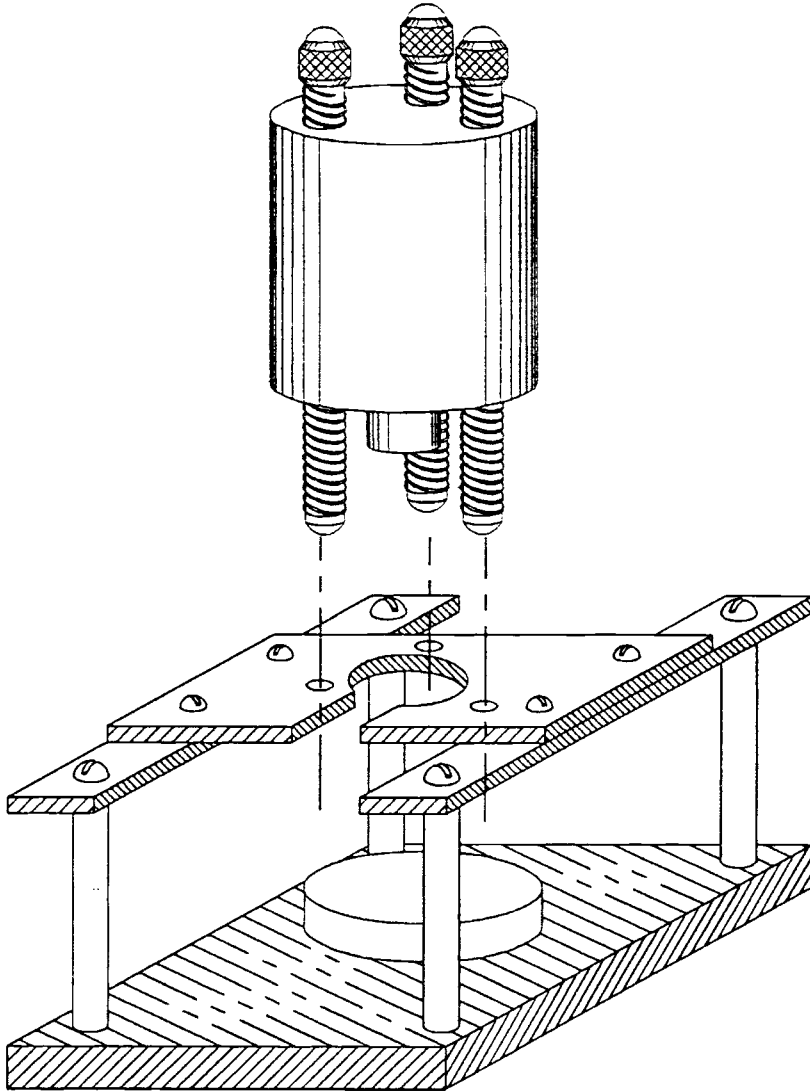


Figure 4. Aluminum rig on wooden base

In order to insure that these findings were not dependent somehow on the material, some scans were made with glass specimens. The legs were lengthened further and the free response produced an even lower resonance of ~ 60 Hz. When the legs were shortened again the resonance changed to ~ 118 Hz. Consistency of the data can be seen by the remarkable resemblance of the spectrum charts in Figures d.25 and d.26. Juang and Pappa (1985) give an exceptional algorithm for obtaining eigenvalues from experimental data.

The StandAlone microscope was placed on the vibration platform of the larger stationary AFM and tested with impulses while scanning glass. Overdamped responses resulted for large impulses, while for average impulses the response was almost unnoticeable. These results are tabulated in d.t.6 and shown in figures d.27 and d.28. The platform should be tested under different scanning conditions such as scan size, scan rate etc., in order to establish more precisely the boundaries of its effectiveness.

Thermal Effects

Some evidence suggests that thermal gradients in the microscope cause the tip to slowly drift over the sample surface. Non repeatability occurs because the tip cannot scan exactly over the same area. Figure d.29. shows how a distinctive feature on a sample appears to move in successive scans taken over a period of two hours. The microscope manufacturer mentioned that two hours is approximately the amount of time that the AFM takes to reach a thermal steady state. Measuring drift over several hours should reveal whether vibrations are causing the AFM to walk or whether thermal gradients are distorting the microscope.

Conclusion

The sources of vibrations and the microscope components that vibrate became evident, and were quantified. Room resonances were identified and a method for mapping them was developed. The following chapter presents some mathematical models that explain why the smaller isolation table is so much more effective than the larger one.

CHAPTER VI

MODELING

One Dimension

The AFM as a vibrating three dimensional system is simple enough to obtain an analytical model. However, the solutions of the modeled equations are complicated enough to require a sophisticated numerical analysis on computer. The full exposition of this model is given in appendix A.

A simplified model could be useful to shed some insight on the interaction of the AFM with various isolation tables. Consider the following diagram of a damped dynamic absorber

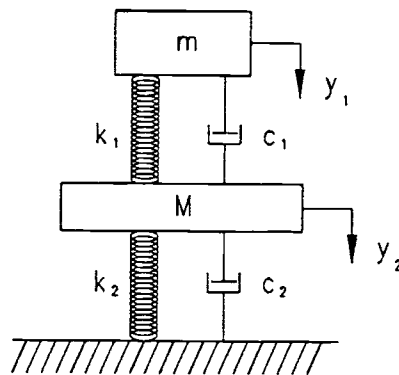


Figure 5. One dimensional dynamic absorber.

The equations of motion are given by

$$m\ddot{y}_1 + k_1(y_1 - y_2) + c_1(\dot{y}_1 - \dot{y}_2) = 0$$

$$M\ddot{y}_2 + k_2 y_2 + k_1(y_2 - y_1) + c_2 \dot{y}_2 + c_1(\dot{y}_2 - \dot{y}_1) = 0$$

If the state of the masses is taken as the position and velocity

$$x_1 = y_1$$

$$x_2 = \dot{y}_1$$

$$x_3 = y_2$$

$$x_4 = \dot{y}_2$$

the equations in state variable form are

$$\dot{x}_1 = x_2$$

$$\dot{x}_2 = \frac{k_1}{m}x_1 - \frac{k_1}{m}x_3 + c_1 x_2 - c_1 x_4$$

$$\dot{x}_3 = x_4$$

$$\dot{x}_4 = \frac{k_2}{M}x_3 + \frac{k_1}{M}x_3 - \frac{k_1}{M}x_1 + c_2 x_4 + c_1 x_4 - c_1 x_2$$

For simplicity let $k_1=1$, and $k_2 < k_1$, say $k_2=1/100$ as it might be for an isolation table. Then

we have

$$\dot{x} = Ax + Bu$$

$$y = Cx + Du$$

where A is the system matrix

$$A = \begin{bmatrix} 0 & 1 & 0 & 0 \\ \frac{1}{m} & c_1 & -\frac{1}{m} & -c_1 \\ 0 & 0 & 0 & 1 \\ -\frac{1}{100M} & -c_1 & \frac{101}{100M} & (c_2 - c_1) \end{bmatrix}$$

if an impulse is given to the mass on top, the input matrix becomes

$$B = \begin{bmatrix} 1 \\ 0 \\ 0 \\ 0 \end{bmatrix}$$

to analyze the response of the mass on top, the output matrix should be

$$C = [1 \ 0 \ 0 \ 0]$$

here the feed through term D can be taken to be zero. These matrices are used with Matlab software to produce a simulation. An impulse input is generated by adding two suitable step functions as shown in the diagram below.

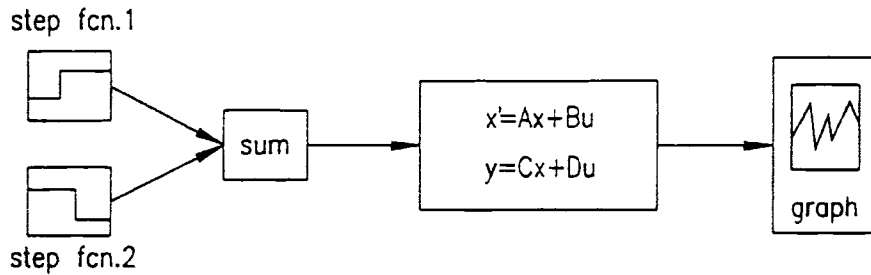


Figure 6. Simulation set up

The simulations for different values of M are shown in figure 7.

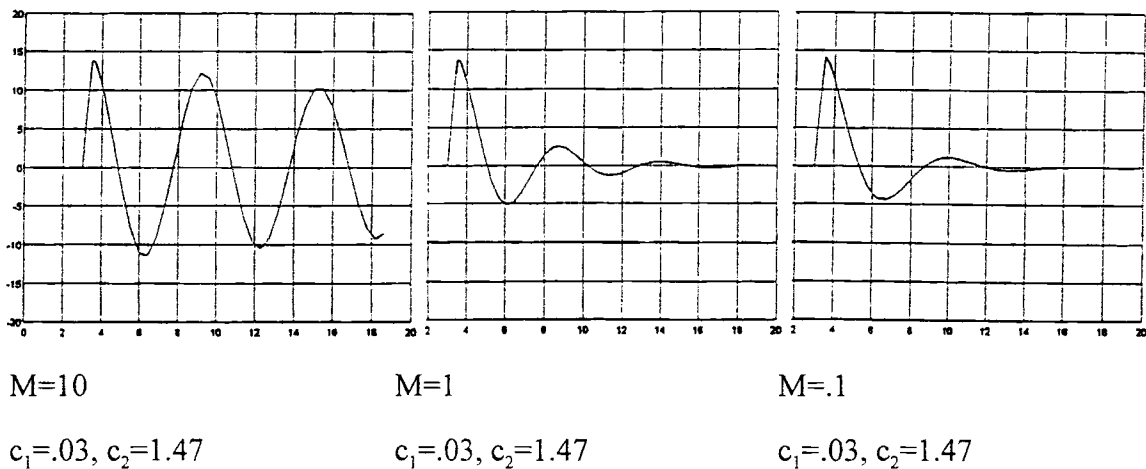


Figure 7. Simulations of one dimensional model

The results are concurrent with experimental findings. When the table is much more massive than the AFM, it does not acquire enough inertia force to become an effective absorber. The model at hand describes bobbing motion, but the system matrix is equivalent for rocking motion, as we might have in the AFM.

Two dimensions

Next consider a four degree of freedom model, which resembles more the AFM on an isolation table.

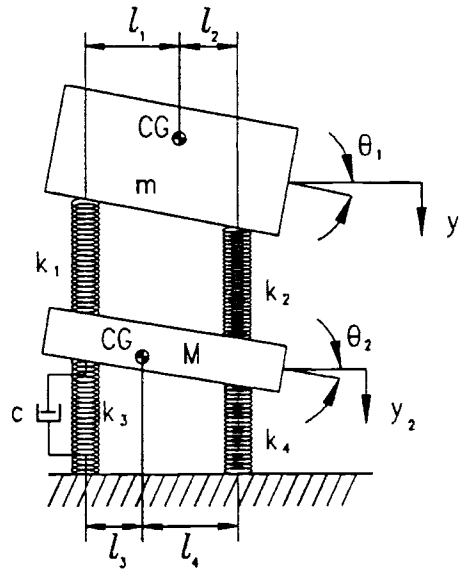


Figure 8. Two dimensional dynamic absorber

The equations of motion are given by

$$m\ddot{y}_1 + k_1(y_1 - y_2 - l_1\theta_1 + l_3\theta_2) + k_2(y_1 - y_2 + l_2\theta_1 - l_4\theta_2) = 0$$

$$J_1\ddot{\theta}_1 - k_1(y_1 - y_2 - l_1\theta_1 + l_3\theta_2)l_1 - k_2(y_1 - y_2 + l_2\theta_1 - l_4\theta_2)l_2 = 0$$

$$M\ddot{y}_2 + k_3(y_2 - l_3\theta_2) + k_1(y_2 - y_1 - l_3\theta_2 + l_1\theta_1) + k_4(y_2 + l_4\theta_2) + k_2(y_2 - y_1 + l_4\theta_2 - l_2\theta_1) + c(\dot{y}_2 - l_3\dot{\theta}_2) = 0$$

$$J_2\ddot{\theta}_2 - k_3(y_2 - l_3\theta_2)l_3 - k_1(y_2 - y_1 - l_3\theta_2 + l_1\theta_1)l_3 - k_4(y_2 + l_4\theta_2)l_4$$

$$- k_2(y_2 - y_1 + l_4\theta_2 - l_2\theta_1)l_4 - c(\dot{y}_2 - l_3\dot{\theta}_2)l_3 = 0$$

for simplicity let $l_1=l_2=l_3=l_4=1$, $k_1=k_2=k/2$, $k_3=k_4=k/200$

the equations become

$$m\ddot{y}_1 + k(y_1 - y_2) = 0$$

$$J_1\ddot{\theta}_1 - k(y_1 - y_2)l = 0$$

$$M\ddot{y}_2 + ky_2 + k(y_2 - y_1) + c(\dot{y}_2 - l\dot{\theta}_2) = 0$$

$$J_2\ddot{\theta}_2 - ky_2l - k(y_2 - y_1)l - c(\dot{y}_2 - l\dot{\theta}_2)l = 0$$

if we take again the state to be the position and velocity

$$x_1 = y_1 \quad x_2 = \dot{y}_1$$

$$x_3 = y_2 \quad x_4 = \dot{y}_2$$

$$x_5 = \theta_1 \quad x_6 = \dot{\theta}_1$$

$$x_7 = \theta_2 \quad x_8 = \dot{\theta}_2$$

The equations can be casted in state space for use with Matlab

$$\dot{x}_1 = x_2$$

$$\dot{x}_2 = -\frac{k}{m} x_1 + \frac{k}{m} x_3$$

$$\dot{x}_3 = x_4$$

$$\dot{x}_4 = \frac{k}{M} x_1 - \frac{101k}{100M} x_3 - c x_4 + c l x_8$$

$$\dot{x}_5 = x_6$$

$$\dot{x}_6 = +\frac{k}{J_1} l x_1 + \frac{k}{J_1} l x_3$$

$$\dot{x}_7 = x_8$$

$$\dot{x}_8 = -\frac{k}{J_2} l x_1 - \frac{101k}{100J_2} l x_3 + c l x_4 - c l^2 x_8$$

The following matrices, derived from the state space equations, can be used with the program given in appendix B to produce simulations.

the system matrix $A =$

$$\begin{bmatrix}
 0 & 1 & 0 & 0 & 0 & 0 & 0 & 0 \\
 -\frac{k}{m} & 0 & \frac{k}{m} & 0 & 0 & 0 & 0 & 0 \\
 0 & 0 & 0 & 1 & 0 & 0 & 0 & 0 \\
 \frac{k}{M} & 0 & -\frac{101k}{100M} & -c & 0 & 0 & 0 & cl \\
 0 & 0 & 0 & 0 & 0 & 1 & 0 & 0 \\
 \frac{k}{J_1} l & 0 & -\frac{k}{J_1} l & 0 & 0 & 0 & 0 & 0 \\
 0 & 0 & 0 & 0 & 0 & 0 & 0 & 1 \\
 -\frac{k}{J_2} l & 0 & \frac{101k}{100J_2} l & cl & 0 & 0 & 0 & -cl^2
 \end{bmatrix}$$

the input matrix

$$B = \begin{bmatrix} 1 \\ 0 \\ 0 \\ 0 \\ 0 \\ 0 \\ 0 \\ 0 \end{bmatrix}$$

the output matrix

$$C = [1 \ 0 \ 0 \ 0 \ 0 \ 0 \ 0 \ 0]$$

The next two graphs show the results of the simulations for $M < m$ and $m < M$ respectively. these results are more instructive than the one dimensional model. The high frequency vibration decreases in amplitude and the low frequency increases when the mass of the AFM exceeds the mass of the isolation table. This is a useful design parameter because of the problems inherent in detecting higher frequency disturbances.

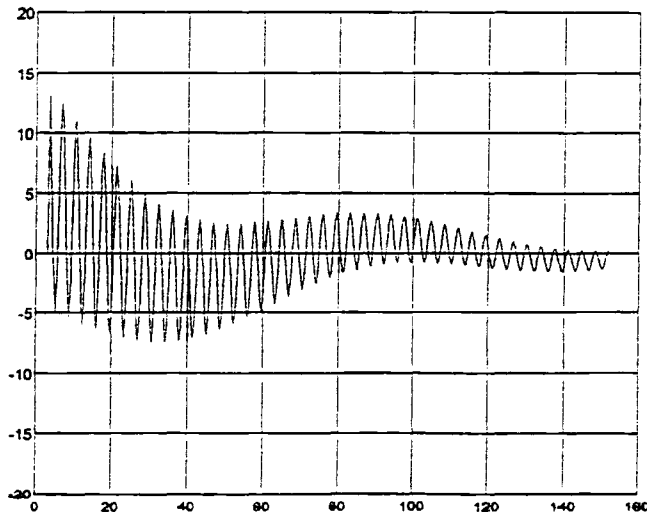


Figure 9.a)

System parameters

$$c=0.1 \quad l=0.8 \quad k=1$$

$$\frac{k_1}{J_1} = 0.004$$

$$\frac{k_1}{J_2} = 0.002$$

$$\frac{k}{m} = 2$$

$$\frac{k}{M} = 1$$

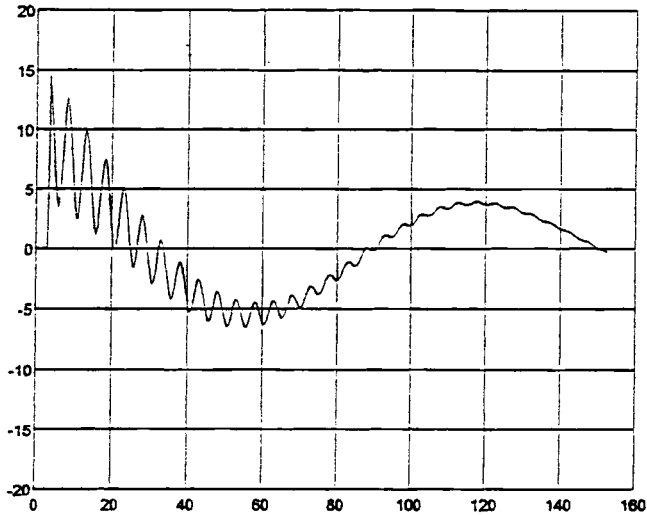


Figure 9.b)

Parameter changes

$$\frac{k}{m} = 0.6$$

Figure 9. Simulation of a two dimensional model

Figure 9 also shows that the high frequency vibration decreases in frequency while the high frequency increases.

Figure 10 shows that the amplitudes but not the frequency decrease to a limit for an increase in coefficient of friction. While figure 11 shows little effect from a change in the mass moments of inertia.

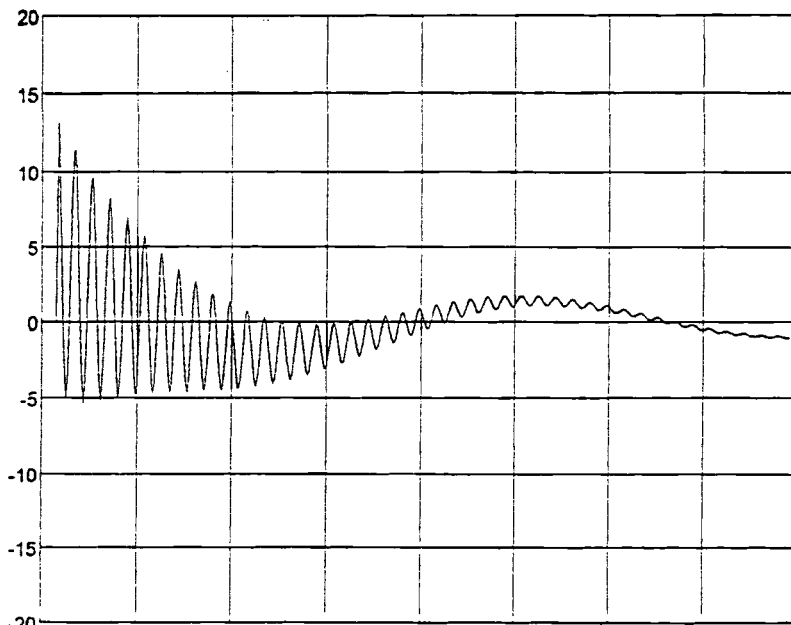


Figure 10.

Parameter changes

$$c = 0.2$$

Figure 11.a)

Parameter changes

$$\frac{k_l}{J_1} = 0.00004$$

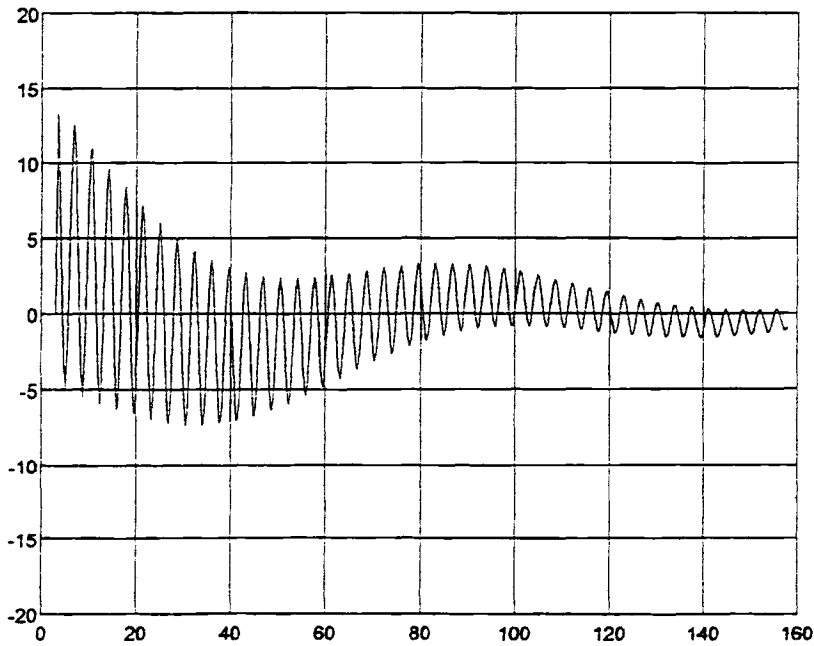
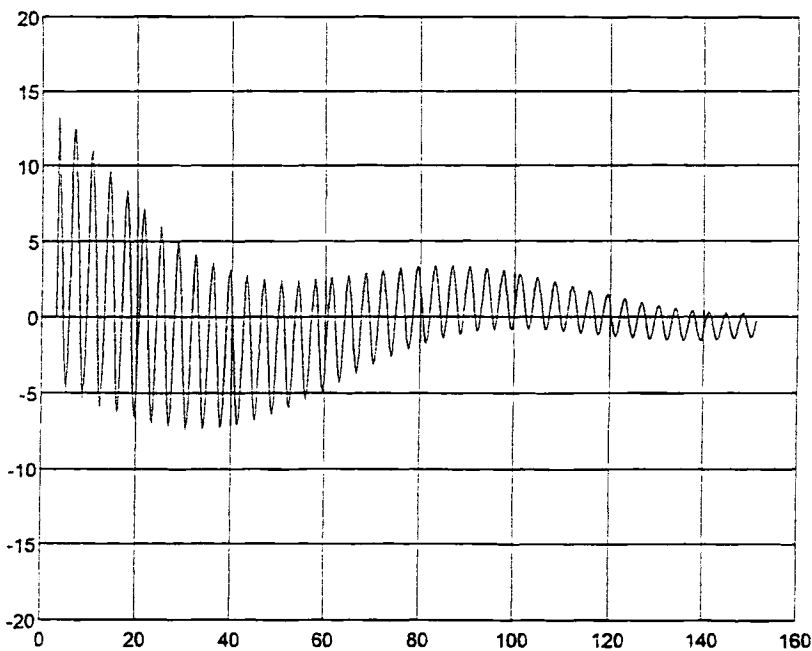


Figure 11.b)

Parameter changes

$$\frac{k_l}{J_2} = 0.00002$$



The damping that results from decreasing the value of l affects exclusively the low frequency vibration (figure 12). This indicates, as one might expect, that this vibration represents the rocking motion, whereas the high frequency is the bobbing motion.

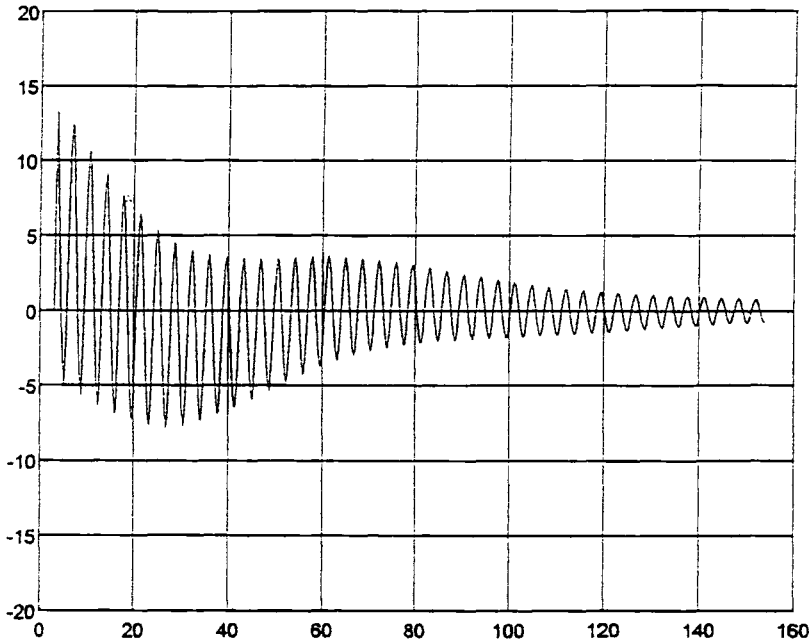


Figure 12.

Parameter changes

$$l=0.01$$

Figure 13 is the simulation of the same system under a sinusoidal driving force on the top mass. Consistent with the free response, both vibrations are damped. It might appear that the transient response is lengthened in 13.b), but a closer look reveals that one graph has more beats of shorter duration.

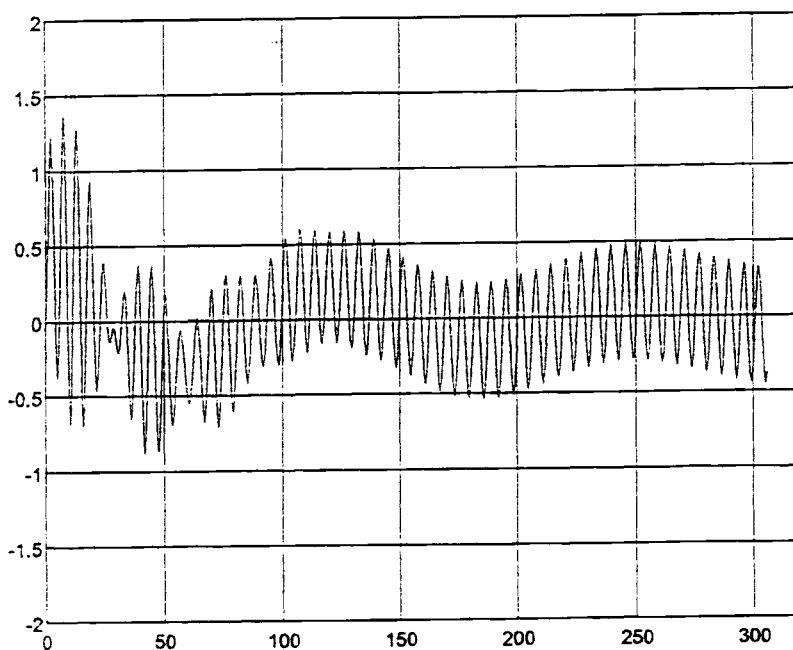


Figure 13.a)

$$m < M$$

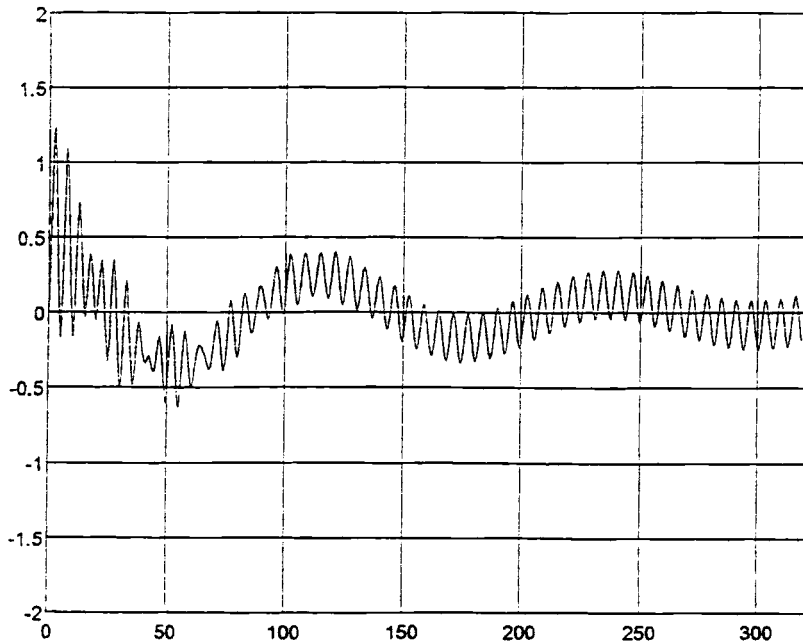


Figure 13.b)

 $m > M$

The simulations and ensuing analysis are superficial because the parameters of the system matrix cannot be altered independently. For example, when k/m changes, k/J must also change. The two dimensional system is a useful model, but the parameters of the matrix A are arbitrary and do not represent the realistic situation. This study is sufficient to indicate a design procedure and to reasonably interpret the different absorption behavior of the two isolation tables in question.

CHAPTER VII

DISCUSSION

Vibration Isolation

The concept for the use of the StandAlone is one of portability. When the sample to be scanned is too large to fit under the Nanoscope, or when it cannot be easily moved, the StandAlone can be placed directly on the surface. For this reason it might be difficult to design an isolation system feasible for all applications. The platform of the Nanoscope is very effective and should be used when possible. The rig currently used for scanning hard disks has four supports that amplify vibrations in the AFM, therefore it should be redesigned. Any new rig design should be given a free response test, and moved to a location of the room where the room modes do not excite AFM or rig resonances. The computer central processing unit, the floppy disk drive and the printer are entirely too noisy, and they should be placed outside of the room. Alternatively an enclosure could be placed around the AFM or rig. The crack under the door allows sound pressure waves to infiltrate, therefore it should be filled. Low frequency noise from the ductwork and the air handler should be suffocated at the vent, perhaps by means of a muffler.

A vacuum enclosure could prevent transmission of acoustic waves. A vacuum chamber could be constructed with glass and silicone, for a negligible cost. While the vacuum pump is the greatest expense, it can be purchased for several hundred dollars. The Physics department may have some pumps which are obsolete but still functional.

An alternative rig design for scanning hard disks is one which holds the microscope in an inverted position. Since gravity is not a factor, an upside down arrangement would reduce the mass on top of the legs and consequently decrease the amplitude of vibrations. Appendix C gives some conceptual designs for isolating the AFM.

The microscope software should be implemented with a feature to view the photodiode signal during a scan. The signal can be viewed only while the microscope is not scanning. The suggested method for maximizing the gains consists of increasing the gains until erratic oscillations appear in the scan and then reducing the gains below that point. However, these oscillations cannot be clearly seen in the scan mode; the photodiode signal gives a clear indication when it oscillates. Such a feature in the software would also be useful for observing vibrations and determining frequency boundaries.

Conclusions

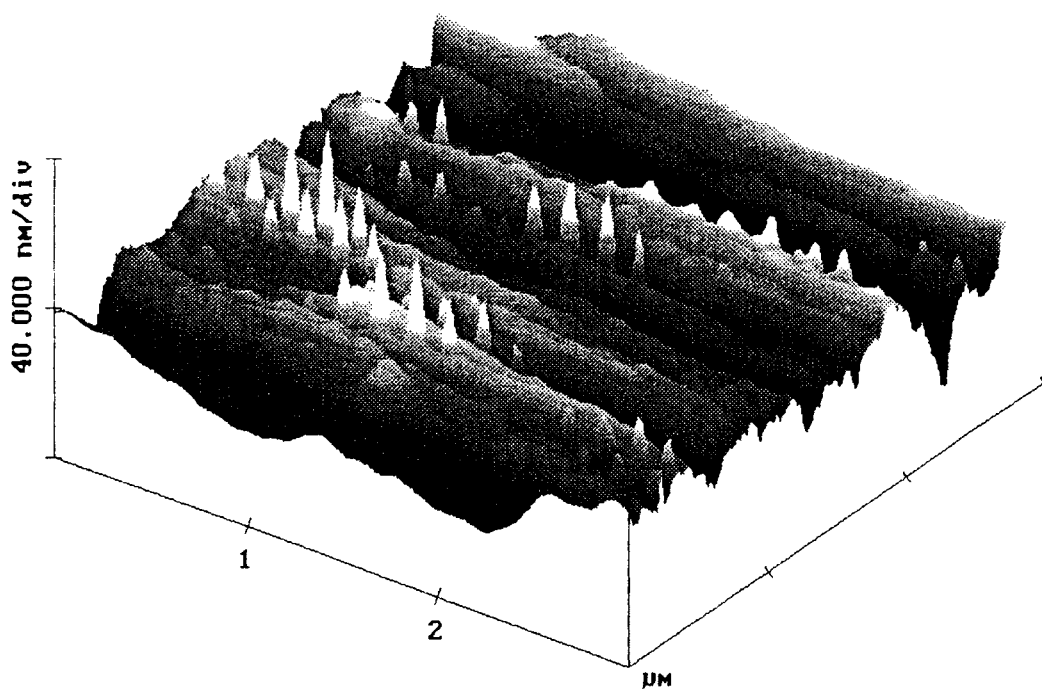
The objective of the study is to stop the spurious data in the AFM. The diagnosis of the existence of unwanted vibrations comes from suspicious scan results and visible disturbances on the scan monitor. The causes are the vibrations through the ground and through the air.

The background is the relation of cantilever tip velocity with wavelength in space, and period in time. The errors are characterized by a constant period in time. The measurements preserve their length with varying scanning speed.

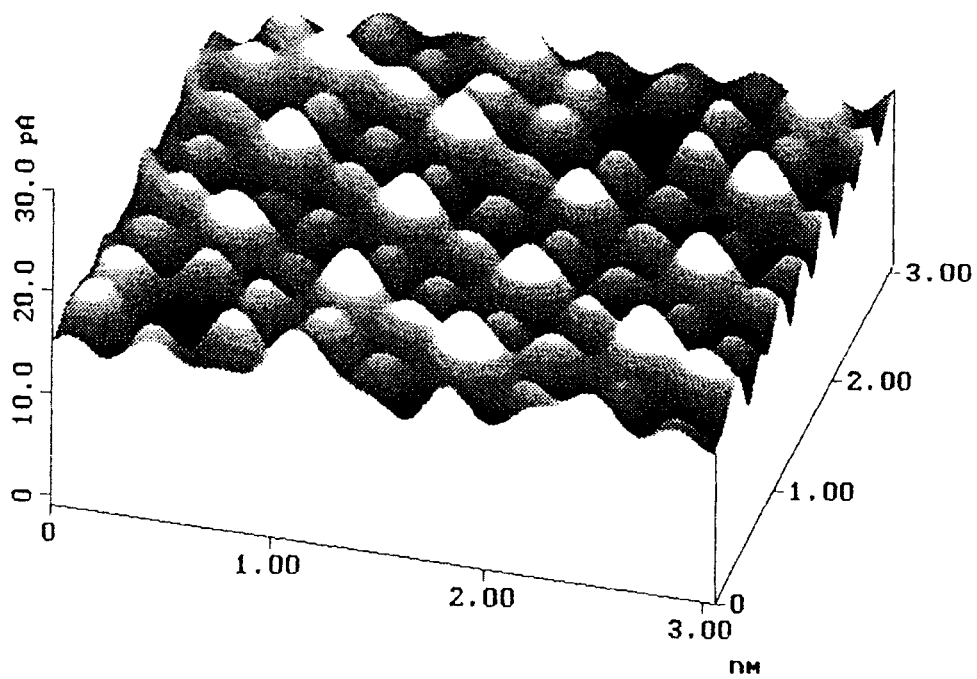
In conclusion, the experimental data shows a direct link between instrument response and extension of the legs. Isolation helps in the form of acoustic enclosure or

small mass isolation tables. Room modes have a selective effect on the frequency and amplitude of the acoustic waves that reach the AFM. Mapping room modes and positioning the AFM appropriately minimizes transmission through the air. Some evidence suggests that thermal fluctuations cause drift. The problem is partially remedied by allowing the system about two hours to reach a steady state.

As a final and personal note: technology has been accused of erecting a barrier between man and nature. There are times, however, when technology brings man closer to nature than he could ever be otherwise (figure 14).



14.a) Vibrations on glass surface



14.b) Iodine atoms

Figure 14. AFM scans

BIBLIOGRAPHY

- Buzdugan, G. (1986). Vibration Measurement. MA: Klumer Academic Publishers.
- Inman, D.J. (1989). Vibration: With Control, Measurement and Stability. New Jersey: Prentice Hall.
- Juang, J-N. Pappa, R.S. (1985). "An Eigensystem Realization Algorithm for Modal Parameter Identification and Model Reduction." AIAA Journal of Guidance, Control, and Dynamics. 8:620-627.
- Macinante, J.A. (1984). Seismic Mountings for Vibration Isolation. New York: Wiley & Sons.
- Tiersen, H.F. (1969). Linear Piezoelectric. Plate Vibration: Elements of the Linear Theory of Piezoelectricity and the Vibrations of Piezoelectric Plates. New York: Plenum Press.

APPENDIXES

APPENDIX A

AFM MODEL

The AFM consists of a mass supported by three screws arranged equilaterally. Because one of the screws has different threads, its stiffness will be different. Vibrations can occur from bending, twisting, rocking, and bobbing.

We can consider r , $\theta_{1,2}$, $\varphi_{1,2}$ as generalized coordinates for the bobbing, rocking, and the bending motions.

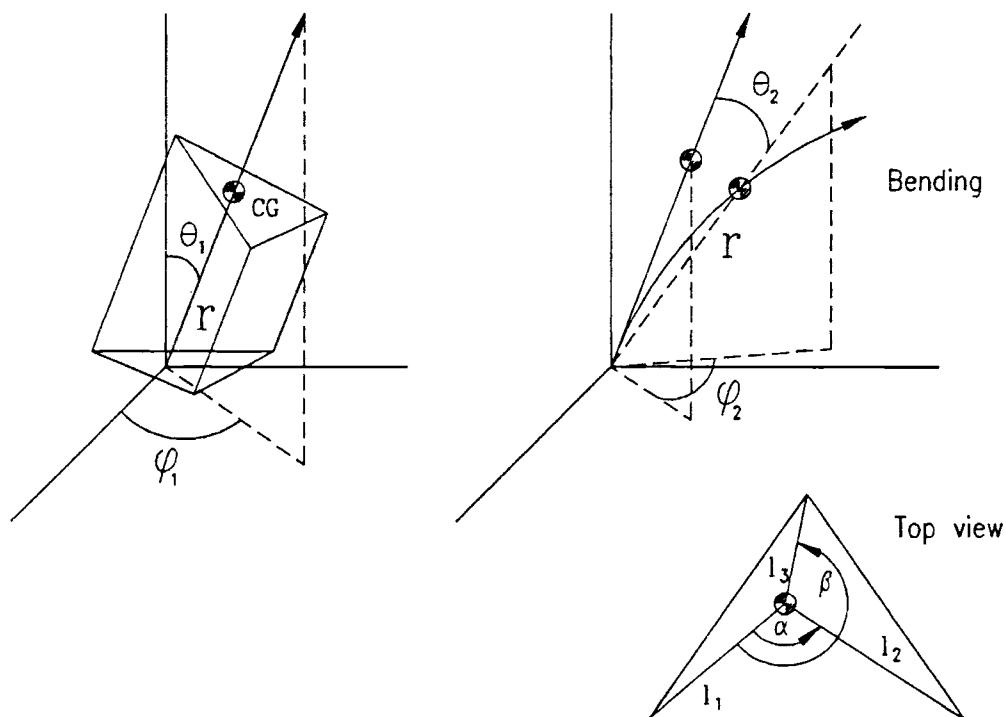


Figure A1. Motions of the center of mass

Therefore we have three degrees of freedom from the bobbing and rocking motions, and two degrees of freedom from the bending motion. Torsion is neglected because it has comparatively little effect on the vertical displacement. If we let r, θ, φ be the coordinates of the center of mass, subject to some constraint of $\theta_{1,2}, \varphi_{1,2}$, we have:

$$T = \frac{1}{2} m (\dot{r}^2 + r^2 \dot{\theta}^2 + r^2 \sin^2 \theta \dot{\varphi}^2)$$

$$\begin{aligned}
 V = & \frac{1}{2} k_1 \{ h + [l_1 \sin \theta_1 \sin \varphi_1] \}^2 & k_1 \approx \frac{EA}{h} & \text{for a rod under axial compression} \\
 & + \frac{1}{2} k_1 \{ h - [l_2 \sin \theta_2 \sin(\varphi_2 + \alpha)] \}^2 \\
 & + \frac{1}{2} k_1 \{ h - [l_3 \sin \theta_3 \sin(\varphi_3 + \beta)] \}^2 \\
 & + \frac{1}{2} k_2 (r \sin \theta_1)^2 & k_2 \approx \frac{3EI}{h^3} & \text{for a cantilever with an end load} \\
 & + mg(h - r \cos \theta) \sin \theta
 \end{aligned}$$

where h is the unstretched length of the legs and of the center of gravity. The gravitational potential energy term is orthogonal to the legs, because the component in the direction of the legs is compensated by a compression of those legs. The remaining energy is dissipated, where structural damping is predominant. For the types of materials used here the energy dissipated is proportional to a power of displacement between 2 and 3.

$$\begin{aligned}
 T = & C_1 \{ h + [l_1 \sin \theta_1 \sin \varphi_1] \}^n \\
 & + C_1 \{ h - [l_2 \sin \theta_2 \sin(\varphi_2 + \alpha)] \}^n \\
 & + C_1 \{ h - [l_3 \sin \theta_3 \sin(\varphi_3 + \beta)] \}^n \\
 & + C_2 (r \sin \theta_1)^n
 \end{aligned}$$

In our choice of coordinates θ, φ , can be expressed in algebraic terms of $\theta_{1,2}$ and $\varphi_{1,2}$, the constraints are therefore holonomic. Then we could consider all coordinates generalized and use the method of undetermined multipliers. If the equations of constraint are:

$$f(\theta, \varphi_1, \varphi_2, \theta_1, \theta_2) = 0$$

$$g(\varphi, \varphi_1, \varphi_2, \theta_1, \theta_2) = 0$$

Lagrange's equations become:

$$\sum_{i=1}^7 \frac{d}{dt} \left(\frac{\partial}{\partial \dot{q}_i} T \right) - \frac{\partial}{\partial q_i} T - \frac{\partial}{\partial q_i} V - \frac{\partial}{\partial q_i} D - \lambda_1 \frac{\partial}{\partial q_i} f - \lambda_2 \frac{\partial}{\partial q_i} g = 0$$

This will yield seven equations and nine unknowns, plus two equations of constraint.

The system can be linearized, simplified to seven equations and conditioned to be solved by computer.

APPENDIX B

SIMULATION PROGRAM

The following Matlab program produces a simulation of the system $x'=Ax+Bu$.
 SYS=TOM(T,X,U,FLAG) returns depending on FLAG certain system values given
 time point, T, current state vector, X, and input vector, U.

FLAG indicates the type of output.

FLAG=1, causes TOM to return state derivatives.

FLAG=2, discrete states.

FLAG=3, system outputs.

FLAG=4, next sample time.

FLAG=0, returns a vector, SIZES, which contains the sizes of the state vector
 and other parameters.

```
function [ret,x0,str]=tom(t,x,u,flag);
sys = mfilename;
new_system(sys)
simver(1.2)
if(0 == (nargin + nargout))
    set_param(sys, 'Location', [60,431,563,438])
    open_system(sys)
end;
set_param(sys, 'algorithm', 'RK-45')
set_param(sys, 'Start time', '0.0')
set_param(sys, 'Stop time', '999999')
set_param(sys, 'Min step size', '0.0001')
set_param(sys, 'Max step size', '10')
set_param(sys, 'Relative error', '1e-3')
set_param(sys, 'Return vars', '')
```

```
% Subsystem 'Graph Scope1'.
```

```

new_system([sys, '/', 'Graph Scope1'])
set_param([sys, '/', 'Graph Scope1'], 'Location', [0,0,274,193])

add_block('built-in/Inport',[sys, '/', 'Graph Scope1/x'])
set_param([sys, '/', 'Graph Scope1/x'],...
    'position',[65,55,85,75])

add_block('built-in/S-function',[sys, '/', ['Graph Scope1/S-function
',13,'M-file which plots',13,'lines',13,'']]
set_param([sys, '/', ['Graph Scope1/S-function',13,'M-file which plots
',13,'lines',13,'']],...
    'function name','sfuny',...
    'parameters','ax, color',...
    'position',[130,55,180,75])
add_line([sys, '/', 'Graph Scope1'],[90,65;120,65])
set_param([sys, '/', 'Graph Scope1'],...
    'Mask Display','plot(0,0,100,100,[90,10,10,10,90,9
0,10],[65,65,90,40,40,90,90],[90,78,69,54,40,31,25,10],[77,60,48,4
6,56,75,81,84])',...
    'Mask Type','Graph scope.')
set_param([sys, '/', 'Graph Scope1'],...
    'Mask Dialogue','Graph scope using MATLAB graph wi
ndow.\nEnter plotting ranges and line type.|Time range:|y-min:|y-m
ax:|Line type (rgbw-*):',...
    'Mask Translate','color = @4; ax = [0, @1, @2, @3]
;')
set_param([sys, '/', 'Graph Scope1'],...
    'Mask Help','This block plots to the MATLAB graph
window and can be used as an improved version of the Scope block.
Look at the m-file sfuny.m to see how it works.')
set_param([sys, '/', 'Graph Scope1'],...
    'Mask Entries','160\/-20\ /20\/' 'y-' '\ /')

% Finished composite block 'Graph Scope1'.

set_param([sys, '/', 'Graph Scope1'],...
    'Drop Shadow',4,...
    'position',[360,76,390,114])

add_block('built-in/To Workspace',[sys, '/', 'To Workspace'])
set_param([sys, '/', 'To Workspace'],...
    'mat-name','yout',...
    'position',[285,12,335,28])

add_block('built-in/Clock',[sys, '/', 'Clock'])
set_param([sys, '/', 'Clock'],...
    'position',[165,10,185,30])

add_block('built-in/Step Fcn',[sys, '/', 'Step Fcn'])
set_param([sys, '/', 'Step Fcn'],...
    'Time','3',...
    'After','30',...
    'position',[135,60,155,80])

add_block('built-in/Sum',[sys, '/', 'Sum'])
set_param([sys, '/', 'Sum'],...
    'position',[205,85,225,105])

```

```

add_block('built-in/Step Fcn',[sys,'/','Step Fcn1'])
set_param([sys,'/','Step Fcn1'],...
    'Time','3.5',...
    'After','-30',...
    'position',[135,130,155,150])

add_block('built-in/State-space',[sys,'/','State-space'])
set_param([sys,'/','State-space'],...
    'A','[0 1 0 0 0 0 0 0 ; -2 0 2 0 0 0 0 0; 0 0 0 1 0
0 0 0; 1 0 -1.01 -1 0 0 0 .001; 0 0 0 0 0 0 1 0 0;.004 0 -.004 0 0 0
0 0; 0 0 0 0 0 0 0 1; -.002 0 .002 0 2 .001 0 0 0 -.0001;]')
set_param([sys,'/','State-space'],...
    'B','[1; 0 ;0 ;0 ;0 ;0 ;0 ;0;]',...
    'C','[1 0 0 0 0 0 0 0]',...
    'D','[0]',...
    'X0','[0 0 0 0 0 0 0 0]',...
    'position',[255,80,315,110])
add_line(sys,[320,95;350,95])
add_line(sys,[190,20;275,20])
add_line(sys,[160,70;195,90])
add_line(sys,[160,140;195,100])
add_line(sys,[230,95;245,95])

% Return any arguments.
if (nargin | nargout)
    % Must use feval here to access system in memory
    if (nargin > 3)
        if (flag == 0)
            eval(['[ret,x0,str]=',sys,'(t,x,u,flag);'])
        )
        else
            eval(['ret =', sys,'(t,x,u,flag);'])
        end
    else
        [ret,x0,str] = feval(sys);
    end
end
end

```

APPENDIX C

ISOLATION DESIGNS

The first conceptual design consists of a mount to support the microscope in an inverted position (Figure c.1.). Since gravity is not a factor, the microscope should be able to scan in this position without affecting the results. Since the mass supported by the legs is considerably less, the vibrations should have a higher frequency and lower amplitude. The stand supports the AFM in the desired position and allows adjustment of the screws to bring the sample in contact with the tip. The configuration of the microscope support is inconsequential because the vibrations occur between the tip and the sample.

Figure c.2. gives a design for scanning computer hard discs on an inverted microscope. The disc mount is relatively simple and can be made lightweight. Its design minimizes the protruding length of the legs, causing them to be stiffer. The disk can be turned and moved with a fine adjustment screw, so that the whole surface can be exposed to the tip without moving the microscope.

The last design (Figure c.3.) shows a combination of isolation systems, including a Faraday cage to screen out electromagnetic interference. The glass enclosure is connected to the vacuum pump by way of rubber bellows. The bellows prevent transmission of vibrations from the pump to the glass. The enclosure design is so simple that if constructed carefully it would yield over 90% vacuum.

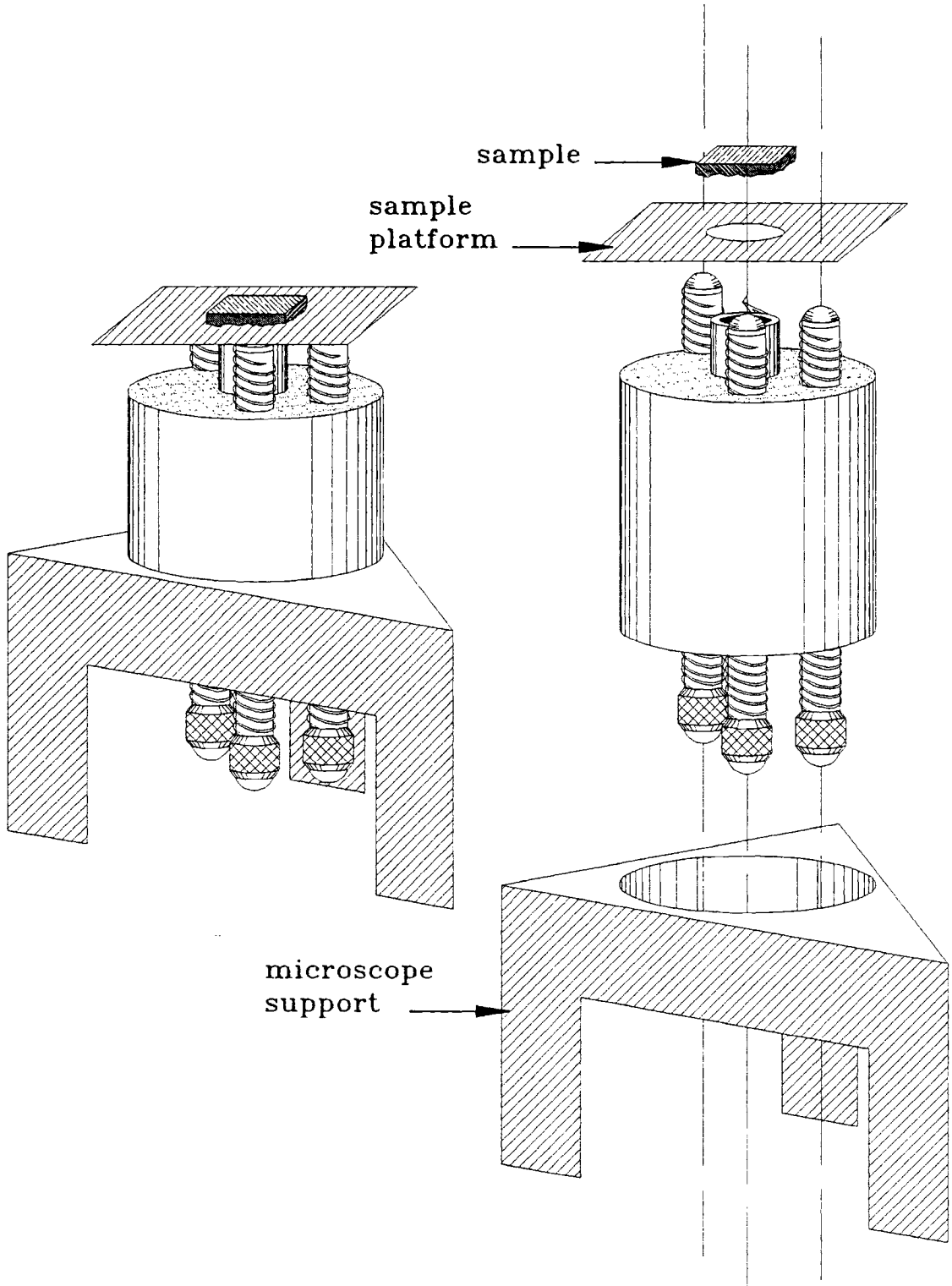


Figure c.1. Conceptual rig design for inverted scanning

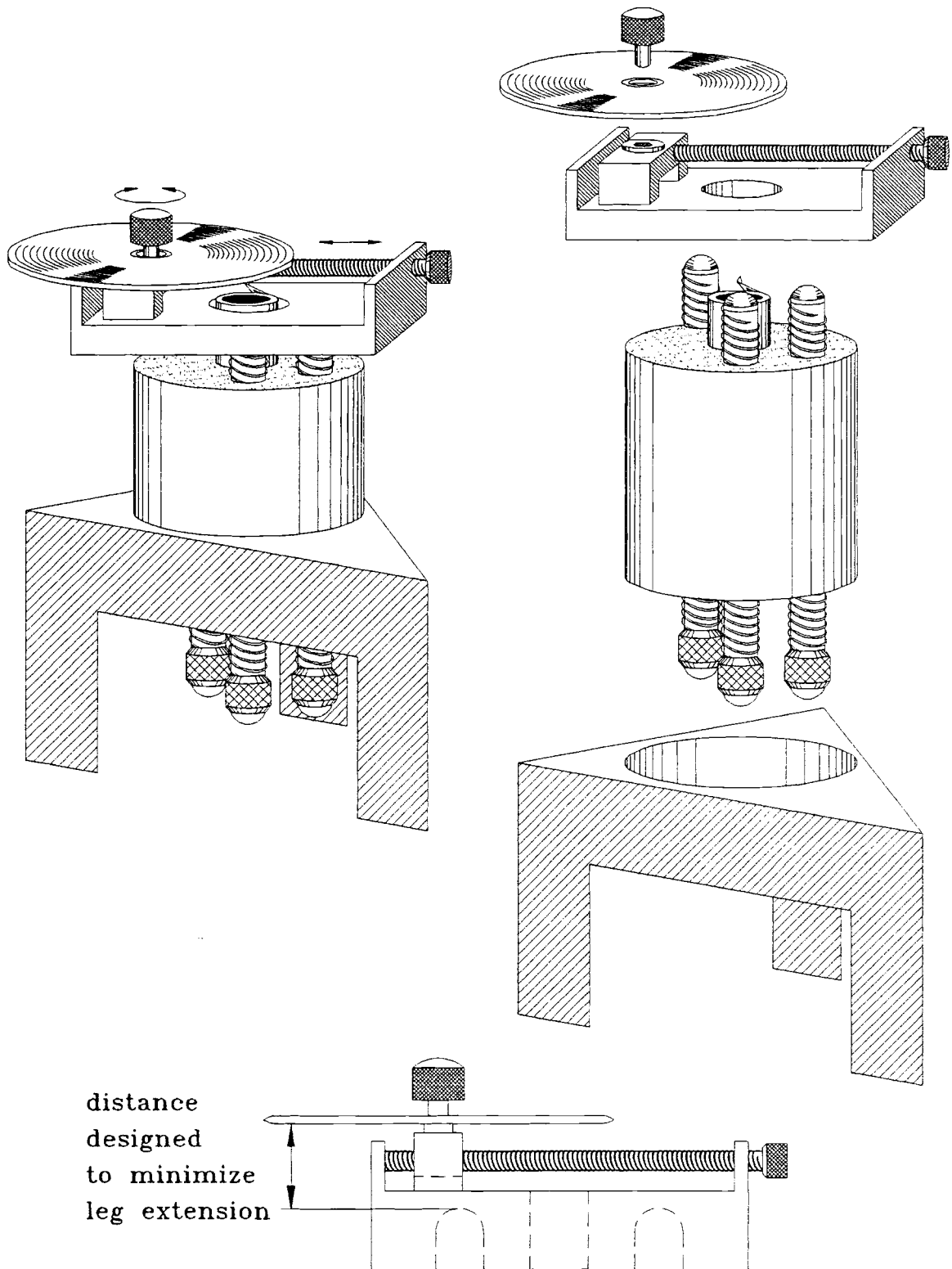
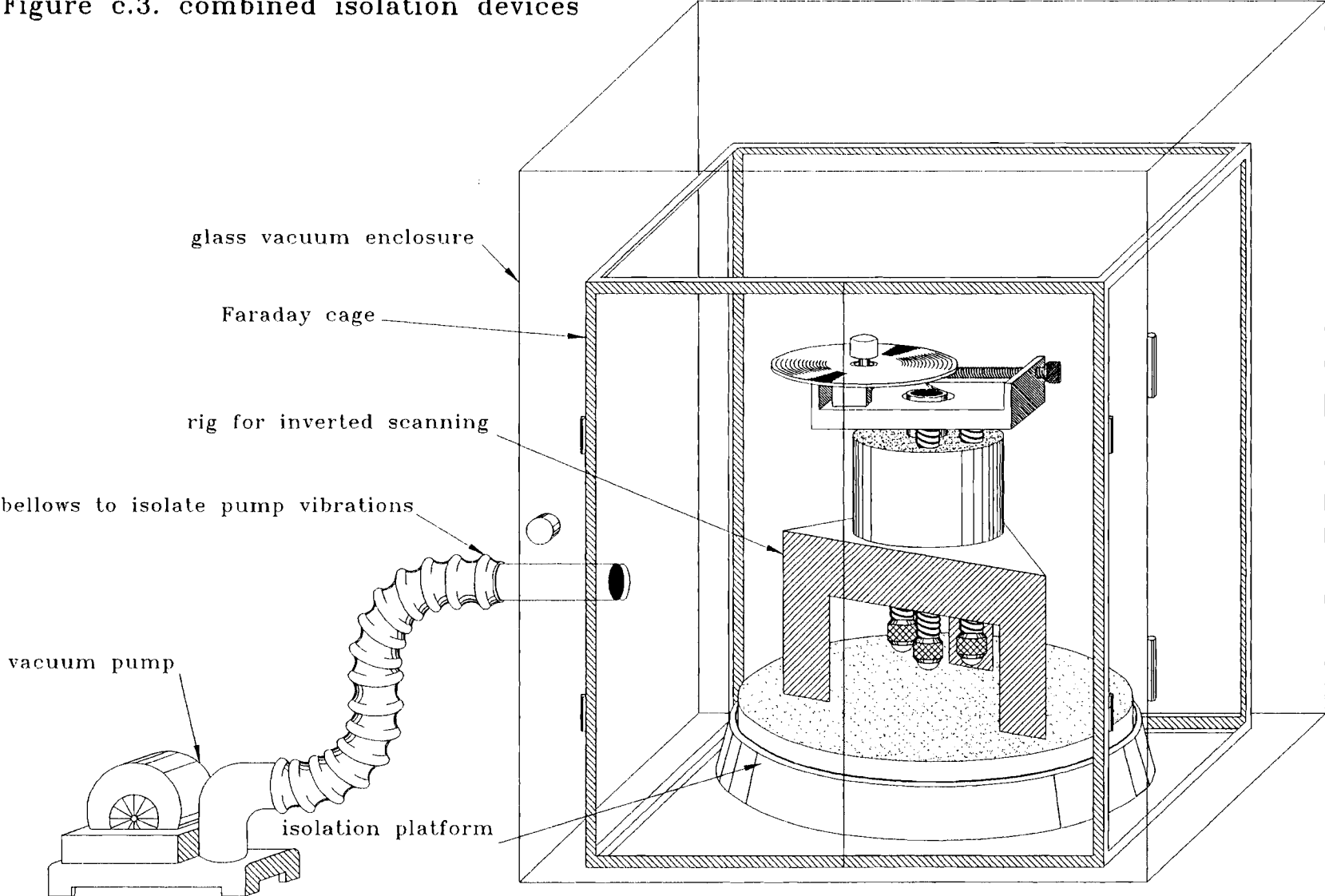


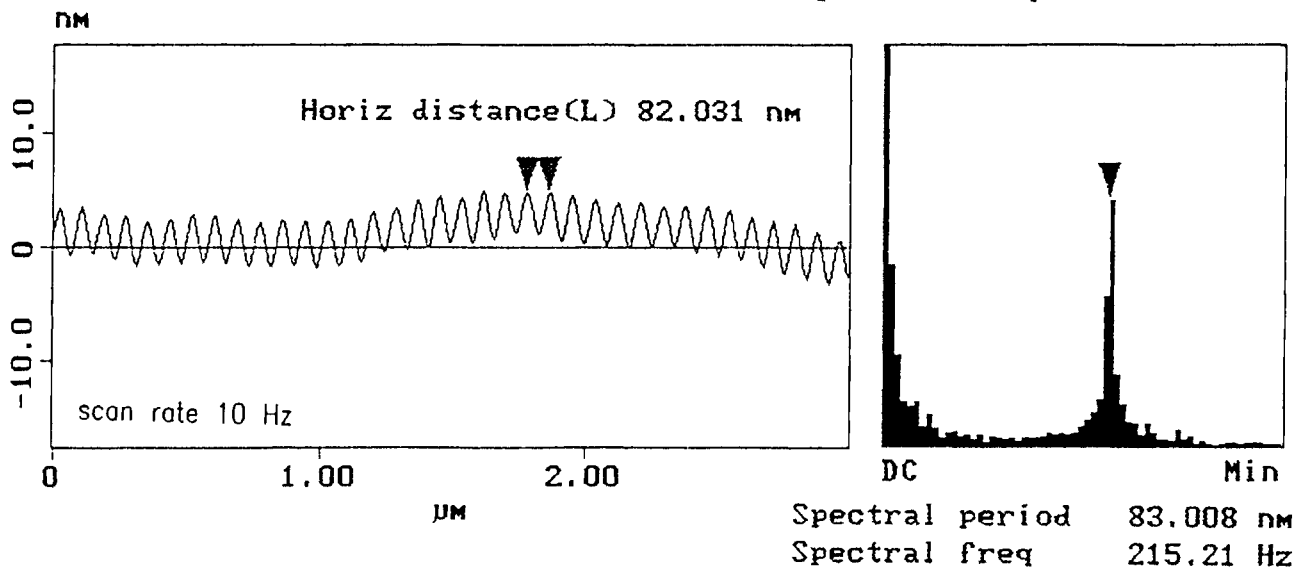
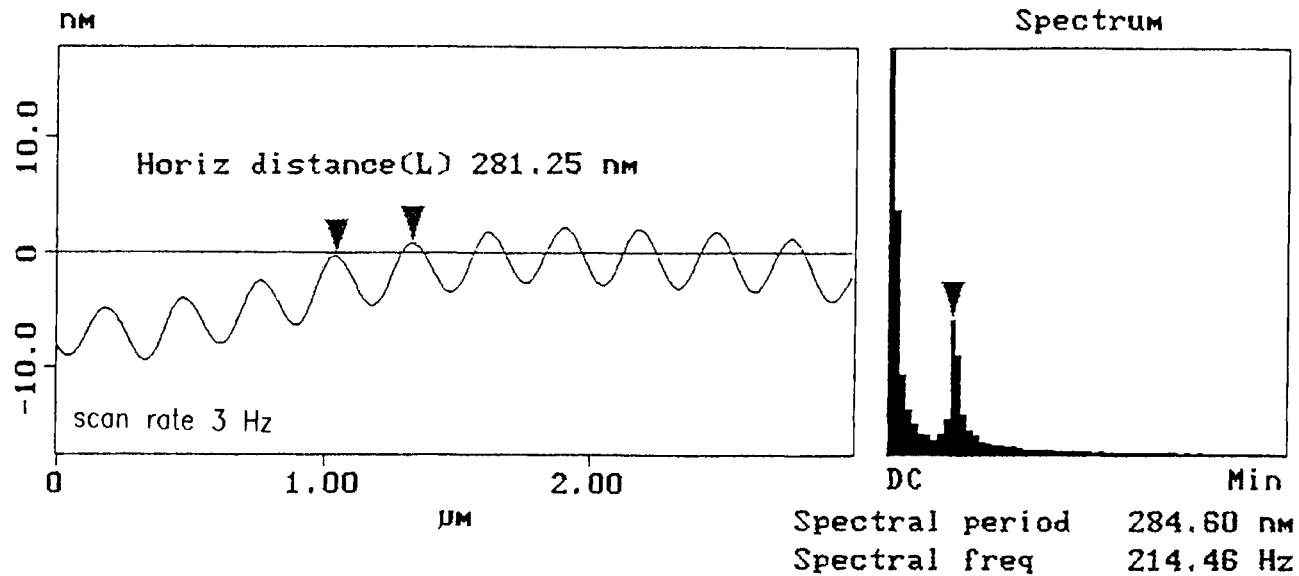
Figure c.2. Conceptual design for inverted scanning of computer hard disks

Figure c.3. combined isolation devices



APPENDIX D
VIBRATION DATA

Figure d.1. Vibrations and scanning speed



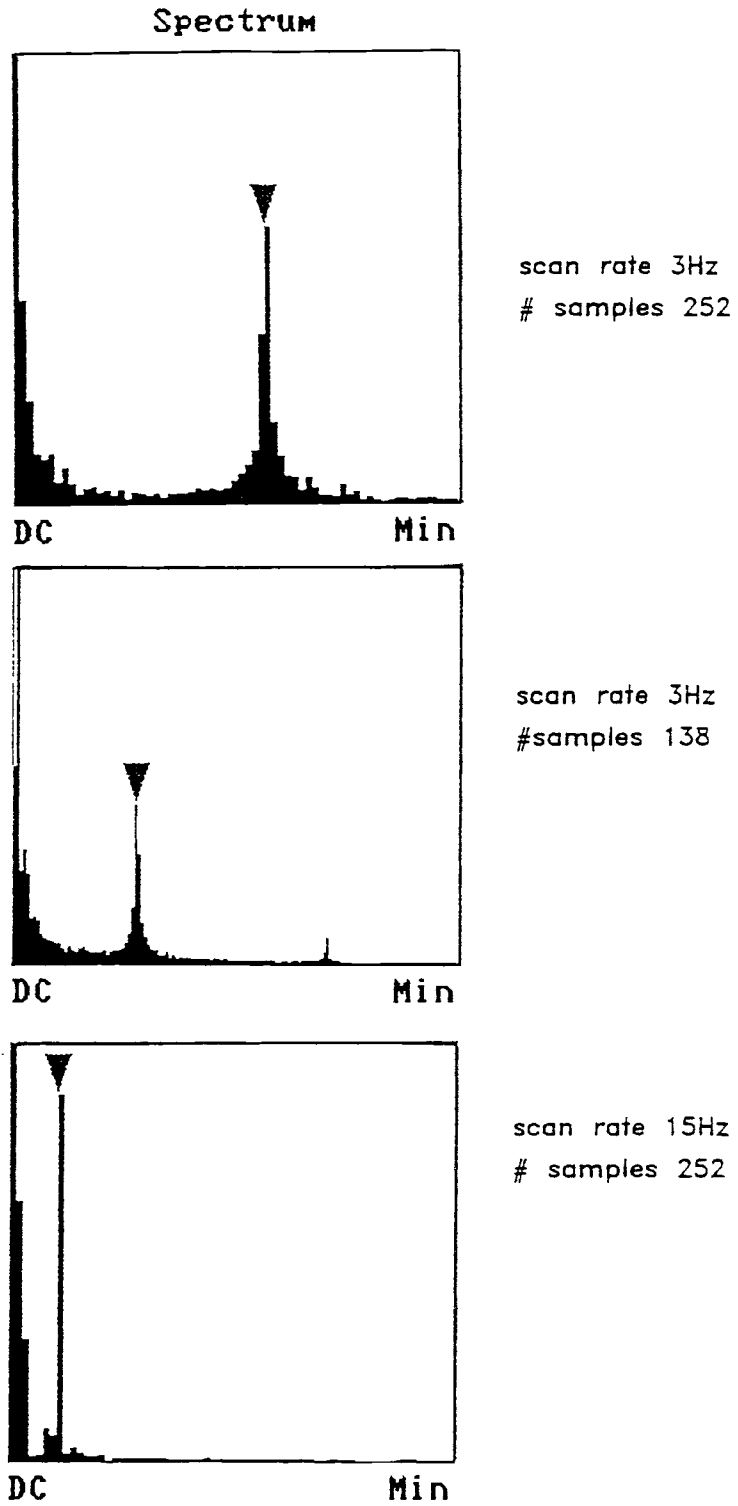


Figure d.2. Surface features

Table d.t.1.

resonances (Hz)			
scan #1.017	scan #1.018	speaker by microscope	speaker in room corner
122.0	188.3	125.0 (beats)	125.0 (beats)
134.0	212.2	165.7	153.5
140.4	224.1	212.2	179.0
144.9	246.6	274.5	204.0
152.4	260.0	296.0	214.0
164.3	266.6	356.0	239.0
176.3	277.9	383.0	257.7
266.0		421.9	285.5
272.0		433.9	298.7
		486.0	354.4
		550.6	391.0
		575.8	435.0
		611.0	460.7
			518.9
			623.0

Table d.t.2.

scan (size $3\mu\text{m}$)		gains					disturbance (amplitude $\sim 80\text{dB}$)
number	rate	type	#samples	integral	proport.		
1.015	3	height	252	.7	1	control scan no disturbance	
1.021	3	height	252	.7	1	21.2Hz, 267.2Hz, 272.9Hz	
1.022	15	height	252	.7	1	21.2Hz (scan too fast for others)	
1.023	10	height	252	.7	1	21.2Hz (scan too fast for others)	
1.024	3	height	252	3.8	5	21.2Hz, 267.2Hz, 272.9Hz	
1.025	3	deflect.	252	3.8	5	21.2Hz, 267.2Hz, 272.9Hz	
1.026	3	deflect.	252	.7	1	21.2Hz, 267.2Hz, 272.9Hz	
1.027	3	height	138	.7	1	21.2Hz, 267.2Hz, 272.9Hz	
1.028	3	height	252	.7	1	21.2Hz, 267.2Hz, 272.9Hz (high cantilever force)	

Table d.t.3.

scan (size $3\mu\text{m}$)			gains			disturbance
number	rate	type	#samples	integral	proport.	
2.000	3	height	512	7	10	none
2.001	15	height	512	7	10	none
2.002	15	height	512	14	20	none
2.003	7	height	512	14	20	none
2.004	20	height	512	21	30	none

Figure d.3. Scan #1.021

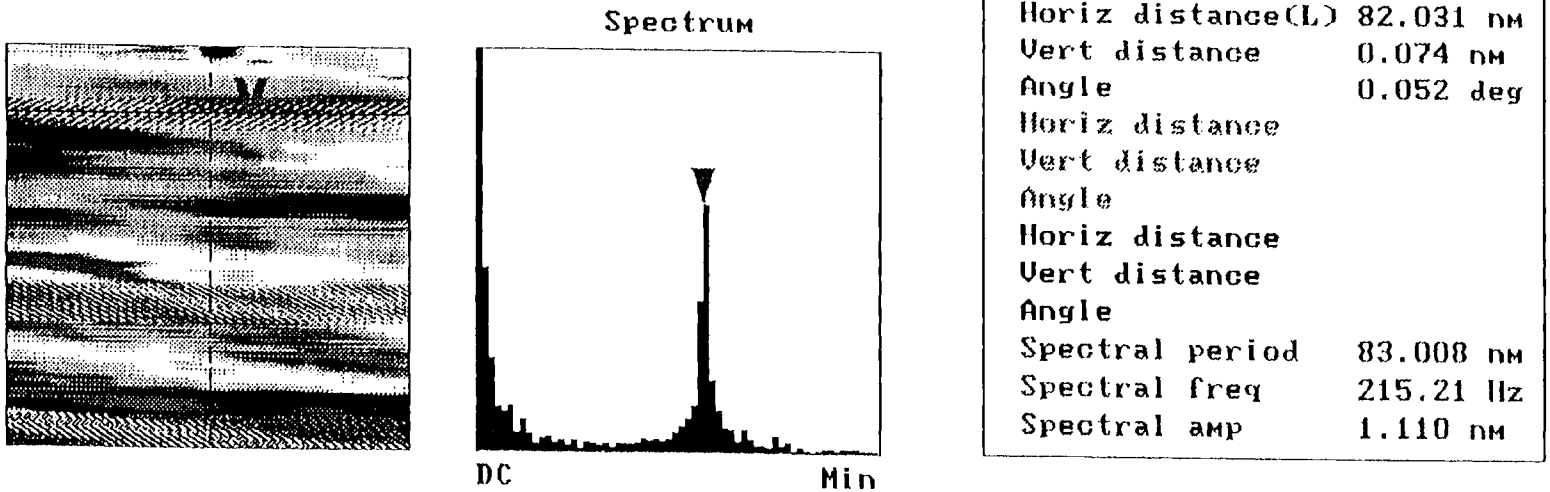
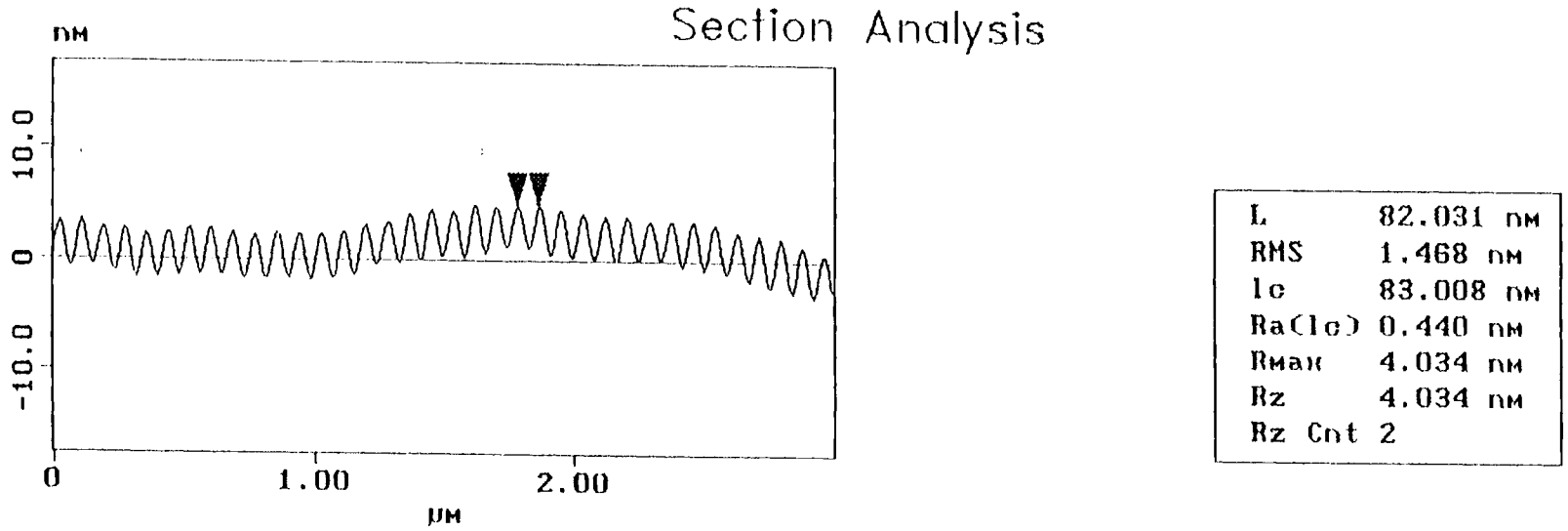
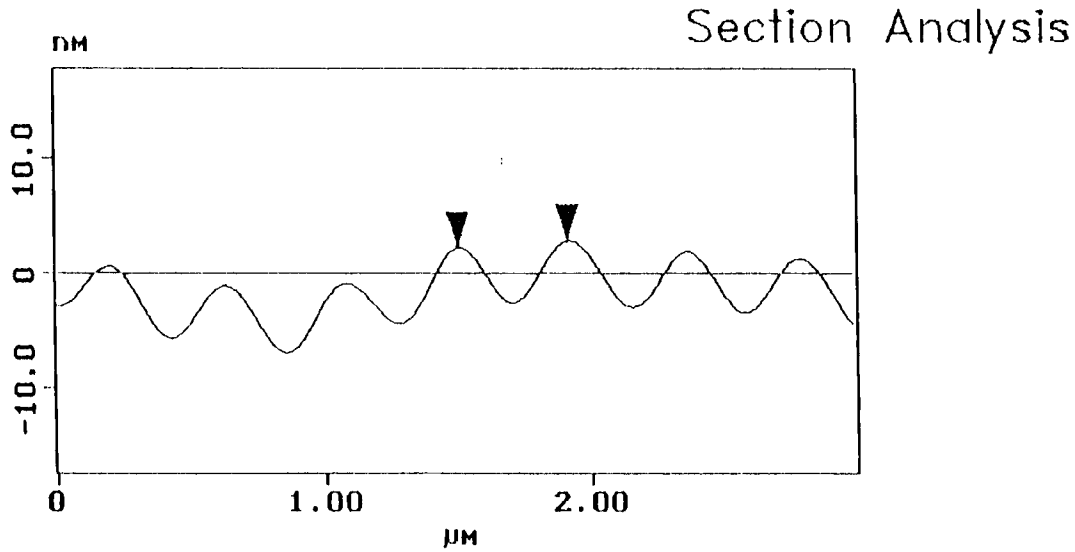
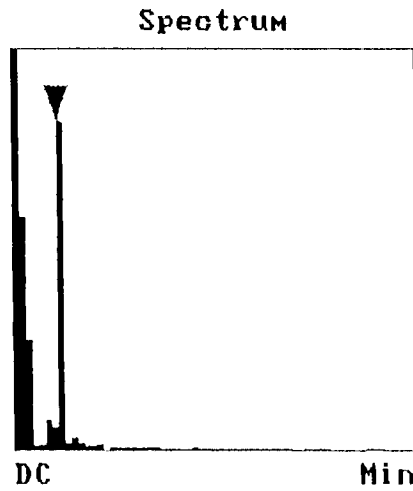
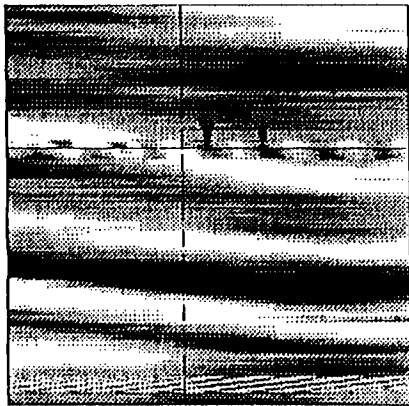


Figure d.4. Scan #1.022



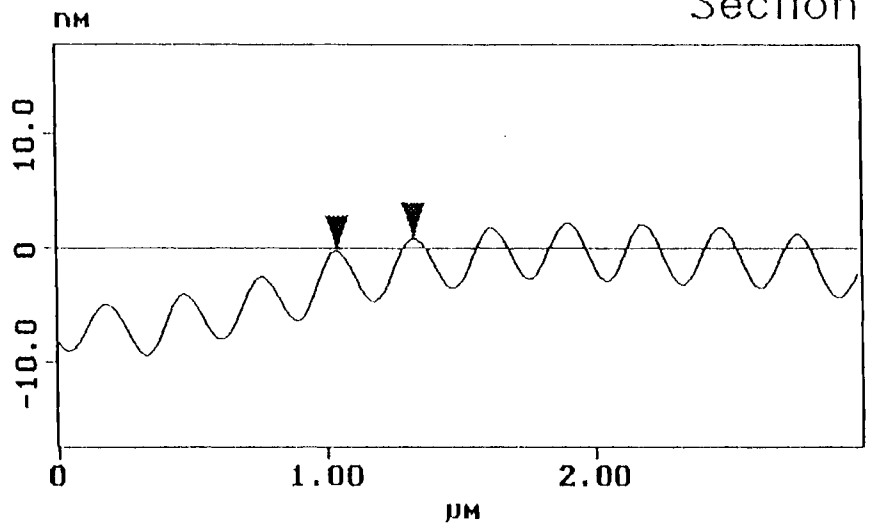
L	410.16 nm
RMS	1.835 nm
lc	426.90 nm
Ra(lc)	0.618 nm
Rmax	5.204 nm
Rz	5.204 nm
Rz Cnt	2



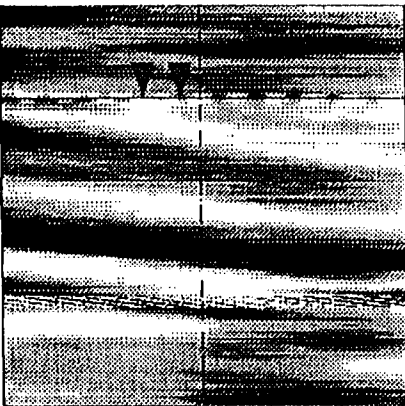
Horiz distance(L)	410.16 nm
Vert distance	0.591 nm
Angle	0.083 deg
Horiz distance	
Vert distance	
Angle	
Horiz distance	
Vert distance	
Angle	
Spectral period	426.90 nm
Spectral freq	214.46 Hz
Spectral amp	1.808 nm

Figure d.5. Scan #1.023

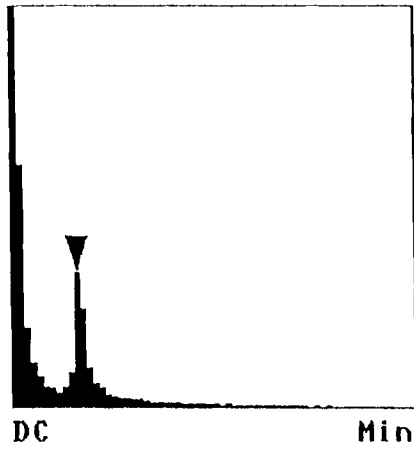
Section Analysis



L	281.25 nm
RMS	1.842 nm
lc	284.60 nm
Ra(lc)	0.568 nm
Rmax	5.402 nm
Rz	5.402 nm
Rz Cnt	2

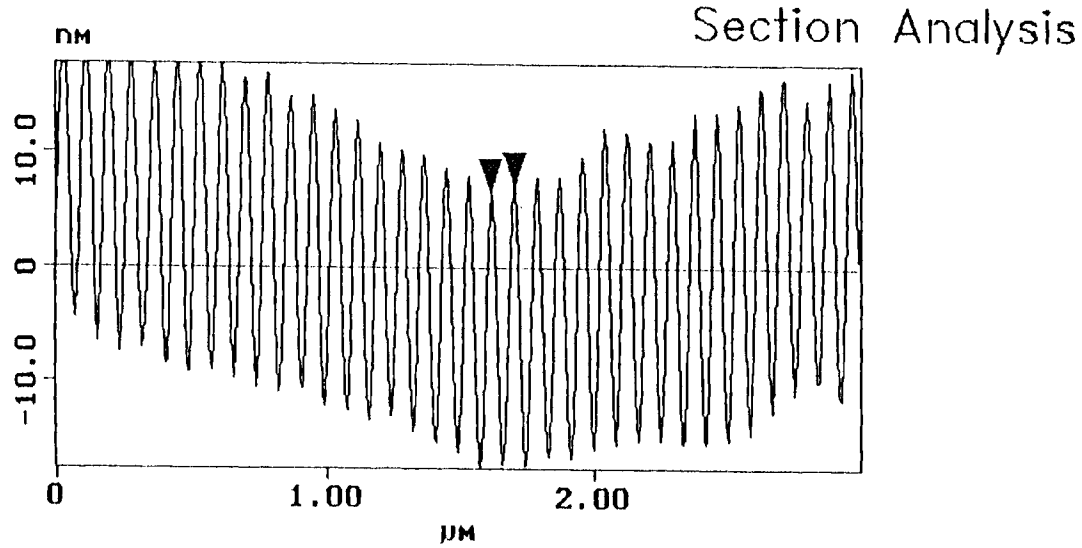


Spectrum

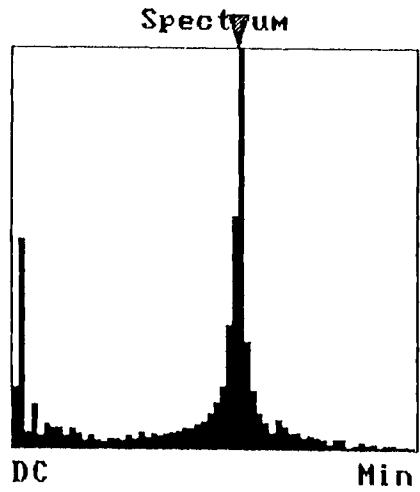
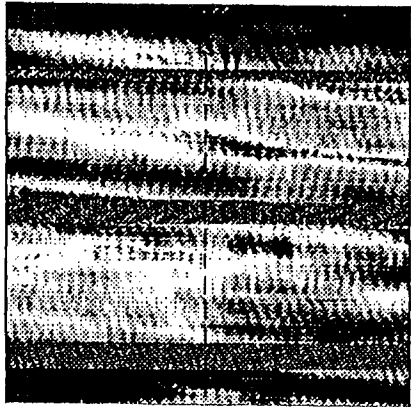


Horiz distance(L)	281.25 nm
Vert distance	1.108 nm
Angle	0.226 deg
Horiz distance	
Vert distance	
Angle	
Horiz distance	
Vert distance	
Angle	
Spectral period	284.60 nm
Spectral freq	214.46 Hz
Spectral amp	1.240 nm

Figure d.6. Scan #1.024



L	82.031 nm
RMS	9.502 nm
lc	83.008 nm
Ra(lc)	2.848 nm
Rmax	26.208 nm
Rz	26.208 nm
Rz Cnt	2



Horiz distance(L)	82.031 nm
Vert distance	0.961 nm
Angle	0.671 deg
Horiz distance	
Vert distance	
Angle	
Horiz distance	
Vert distance	
Angle	
Spectral period	83.008 nm
Spectral freq	215.21 Hz
Spectral amp	7.257 nm

Figure d.7. Scan #1.025

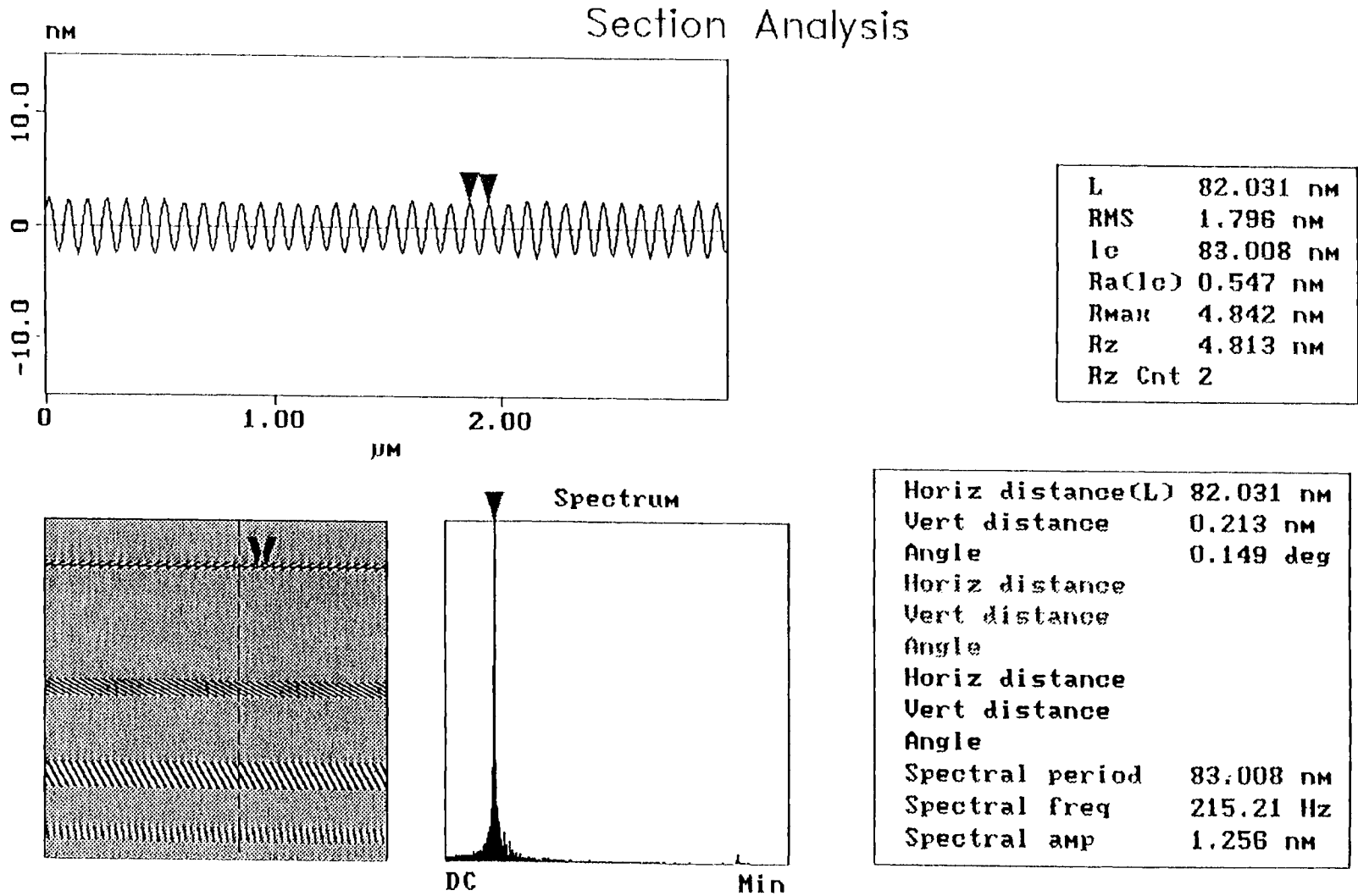
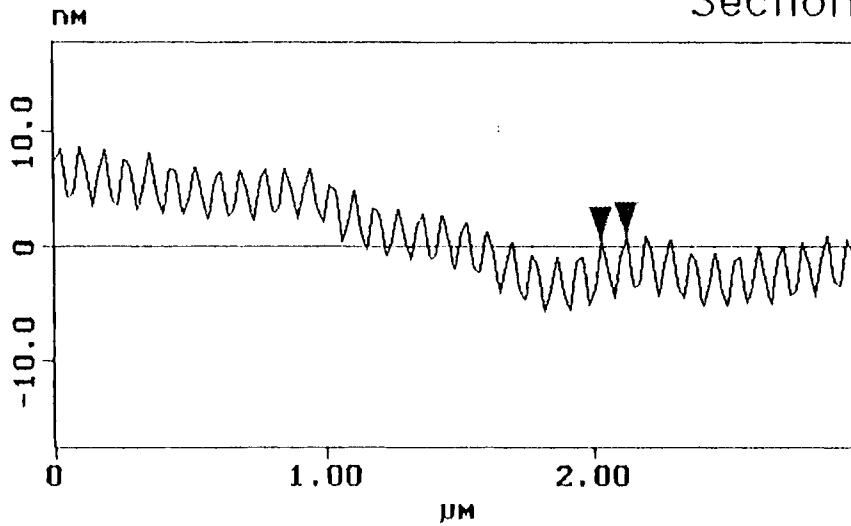


Figure d.8. Scan #1.027

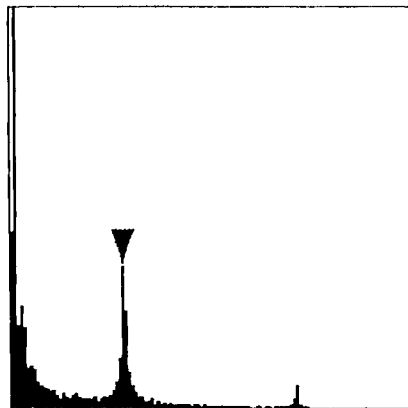
Section Analysis



L	93.750 nm
RMS	1.924 nm
lc	83.847 nm
Ra(lc)	0.462 nm
Rmax	5.507 nm
Rz	5.507 nm
Rz Cnt	2



Spectrum

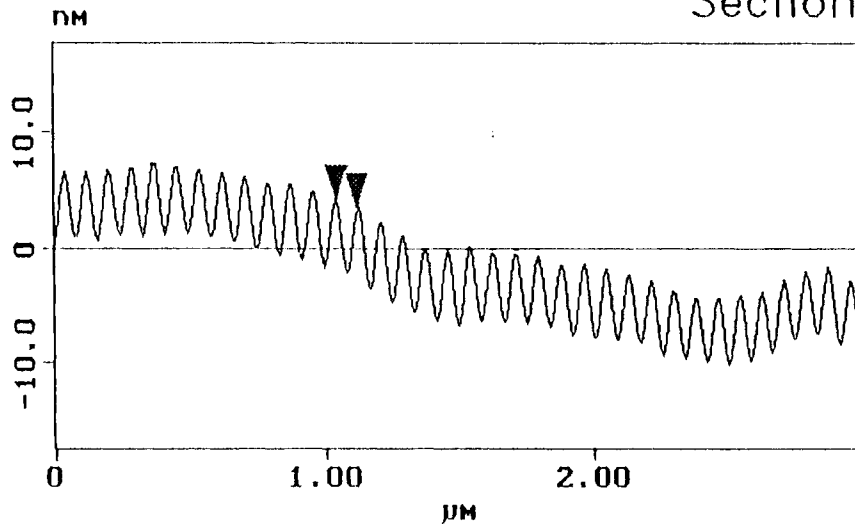


Horiz distance(L)	93.750 nm
Vert distance	0.369 nm
Angle	0.226 deg
Horiz distance	
Vert distance	
Angle	
Horiz distance	
Vert distance	
Angle	
Spectral period	83.847 nm
Spectral freq	213.05 Hz
Spectral amp	1.068 nm

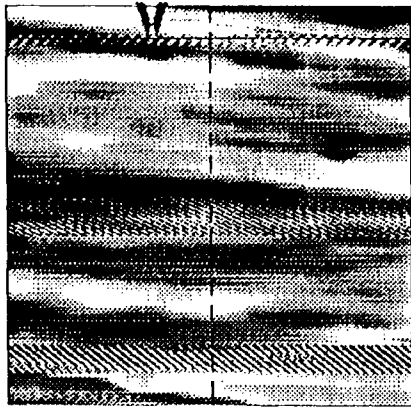
DC Min

Figure d.9. Scan #1.028

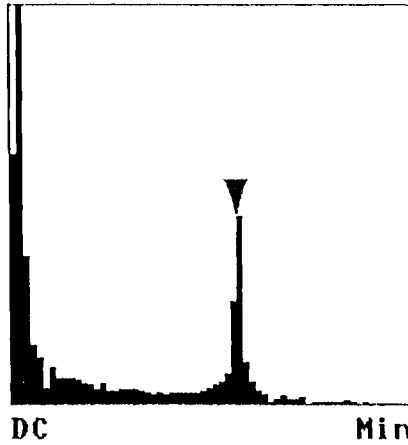
Section Analysis



L	70.313 nm
RMS	2.234 nm
lc	83.008 nm
Ra(lc)	0.665 nm
Rmax	5.957 nm
Rz	5.957 nm
Rz Cnt	2

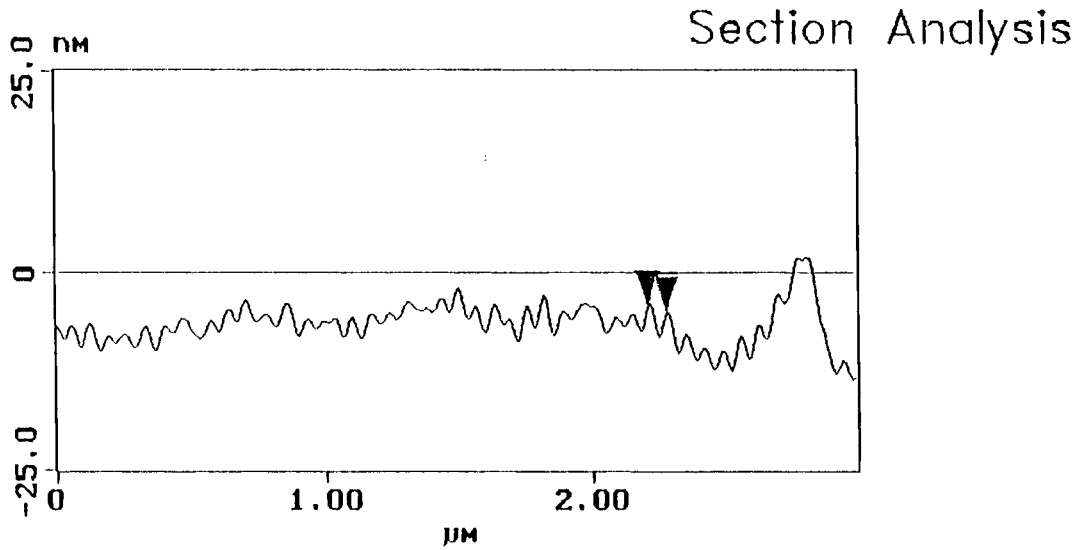


Spectrum

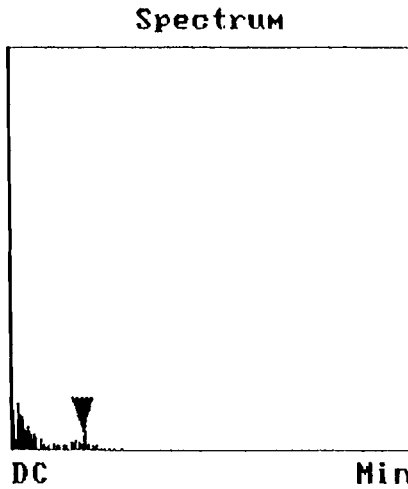
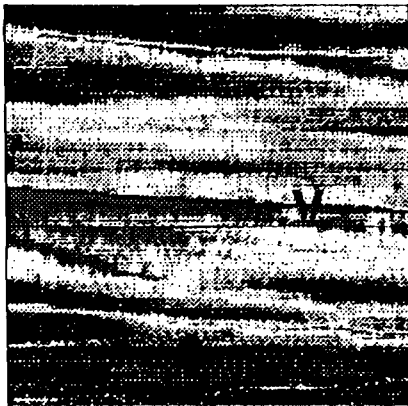


Horiz distance(L)	70.313 nm
Vert distance	0.665 nm
Angle	0.542 deg
Horiz distance	
Vert distance	
Angle	
Horiz distance	
Vert distance	
Angle	
Spectral period	83.008 nm
Spectral freq	215.21 Hz
Spectral amp	1.727 nm

Figure d.10. Scan #2.000

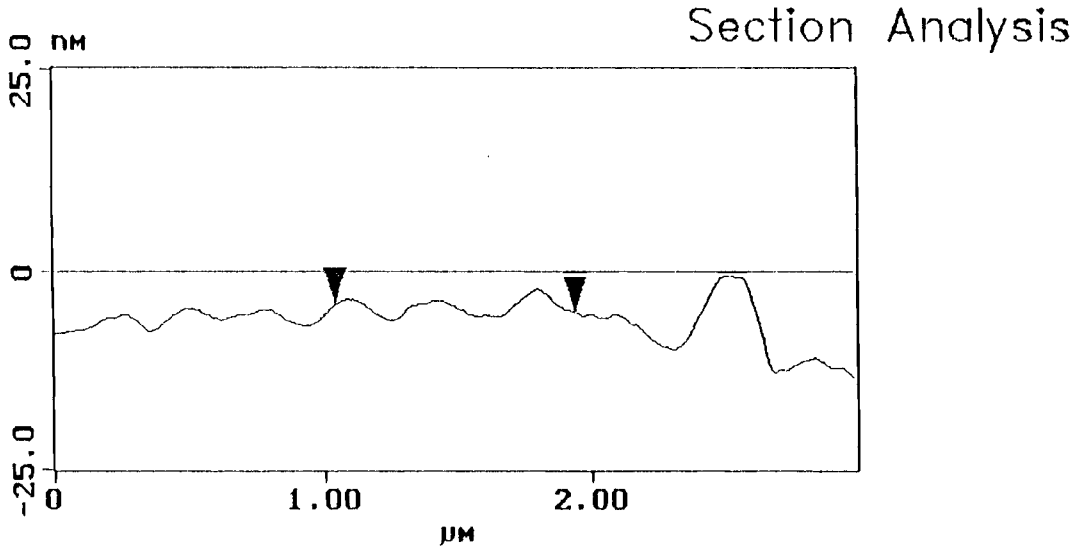


L	70.313 nm
RMS	1.426 nm
lc	66.406 nm
Ra(lc)	0.382 nm
Rmax	4.084 nm
Rz	4.053 nm
Rz Cnt	2

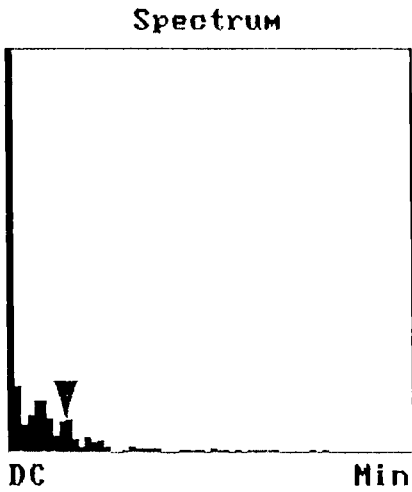


Horiz distance(L)	70.313 nm
Vert distance	0.738 nm
Angle	0.602 deg
Horiz distance	
Vert distance	
Angle	
Horiz distance	
Vert distance	
Angle	
Spectral period	66.406 nm
Spectral freq	275.74 Hz
Spectral amp	0.324 nm

Figure d.11. Scan #2.001

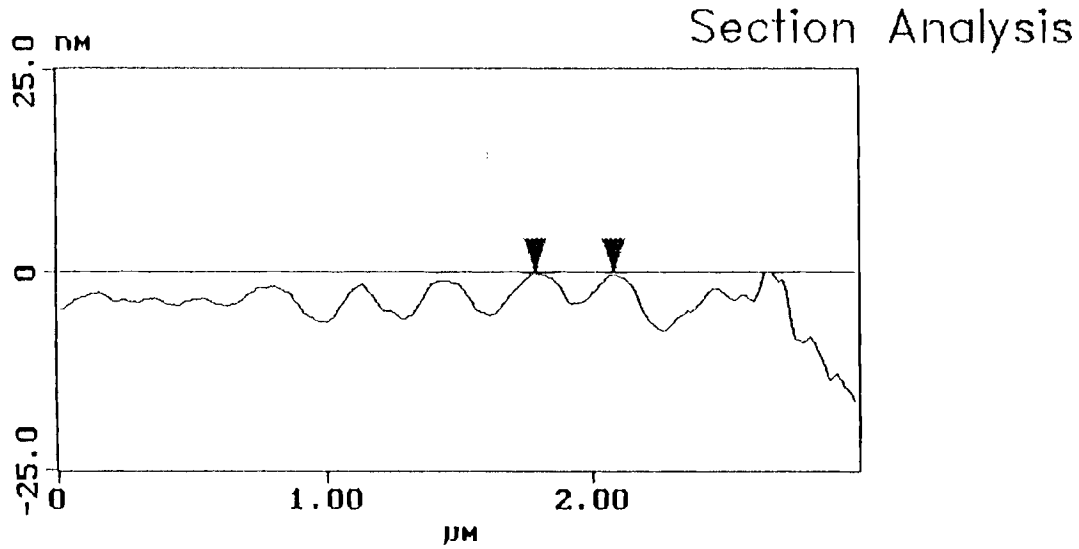


L	896.48 nm
RMS	0.987 nm
lc	332.03 nm
Ra(lc)	0.302 nm
Rmax	3.576 nm
Rz	2.638 nm
Rz Cnt	6

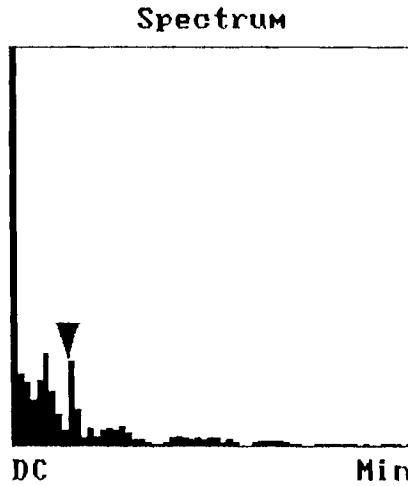


Horiz distance(L)	896.48 nm
Vert distance	1.034 nm
Angle	0.066 deg
Horiz distance	
Vert distance	
Angle	
Horiz distance	
Vert distance	
Angle	
Spectral period	332.03 nm
Spectral freq	275.74 Hz
Spectral amp	0.672 nm

Figure d.12. Scan #2.002



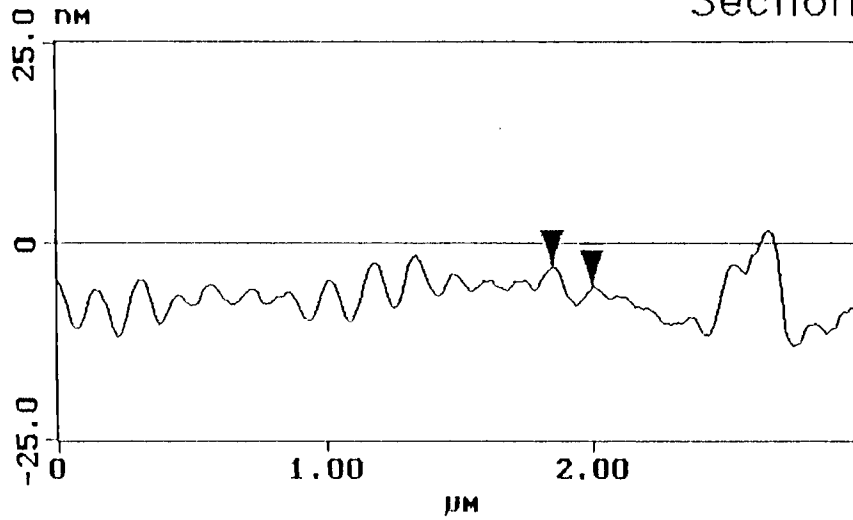
L	292.97 nm
RMS	1.385 nm
lc	332.03 nm
Ra(lc)	0.485 nm
Rmax	4.159 nm
Rz	4.159 nm
Rz Cnt	2



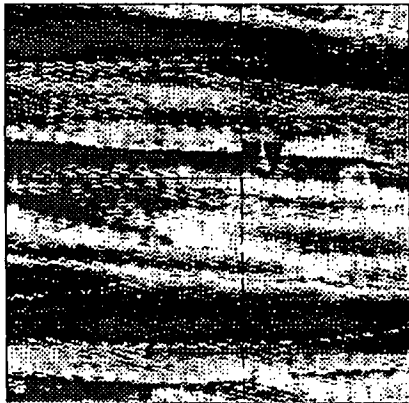
Horiz distance(L)	292.97 nm
Vert distance	0.074 nm
Angle	0.014 deg
Horiz distance	
Vert distance	
Angle	
Horiz distance	
Vert distance	
Angle	
Spectral period	332.03 nm
Spectral freq	275.74 Hz
Spectral amp	1.177 nm

Figure d.13. Scan #2.003

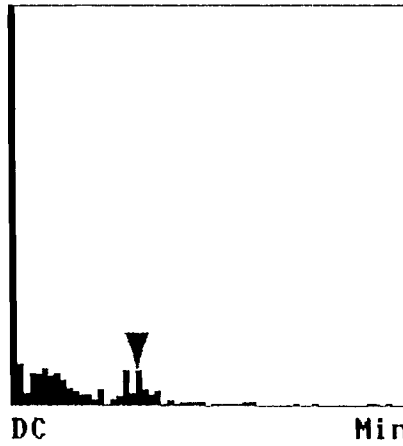
Section Analysis



L	152.34 nm
RMS	1.557 nm
lc	147.57 nm
Ra(lc)	0.384 nm
Rmax	3.928 nm
Rz	3.885 nm
Rz Cnt	2

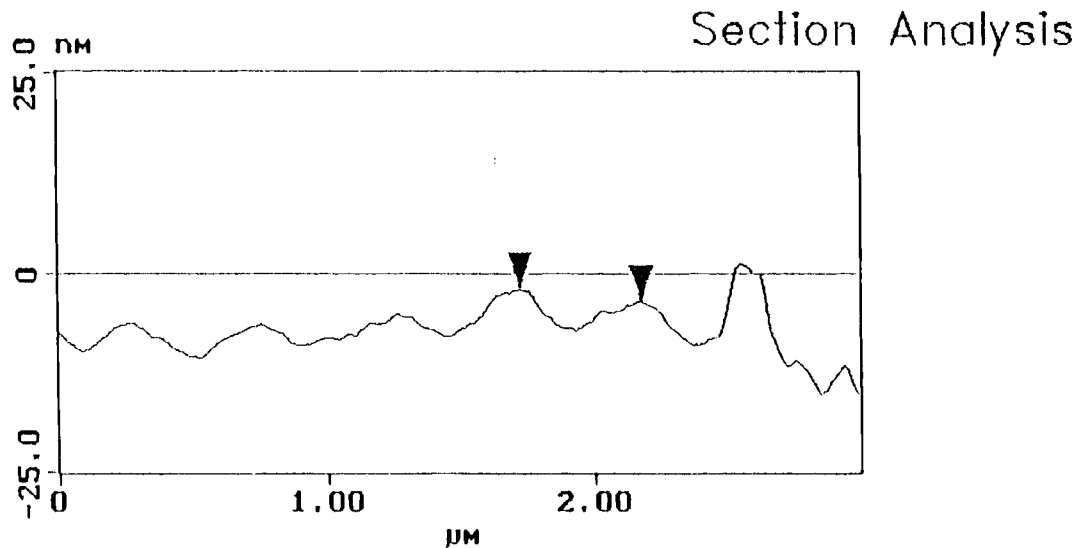


Spectrum

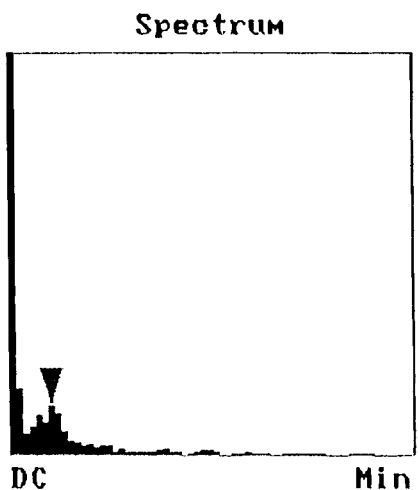
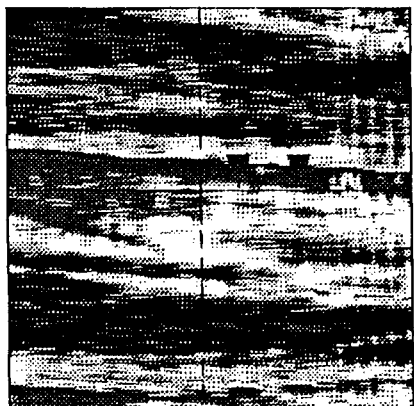


Horiz distance(L)	152.34 nm
Vert distance	2.511 nm
Angle	0.944 deg
Horiz distance	
Vert distance	
Angle	
Horiz distance	
Vert distance	
Angle	
Spectral period	147.57 nm
Spectral freq	275.74 Hz
Spectral amp	0.826 nm

Figure d.14. Scan #2.004



L	451.17 nm
RMS	1.424 nm
lc	459.74 nm
Ra(lc)	0.463 nm
Rmax	5.068 nm
Rz	5.068 nm
Rz Cnt	2



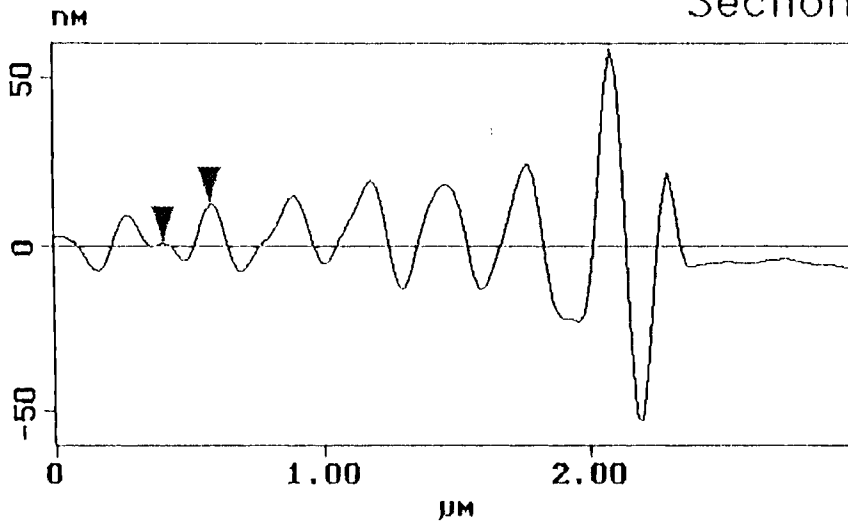
Horiz distance(L)	451.17 nm
Vert distance	1.551 nm
Angle	0.197 deg
Horiz distance	
Vert distance	
Angle	
Horiz distance	
Vert distance	
Angle	
Spectral period	459.74 nm
Spectral freq	265.52 Hz
Spectral amp	1.202 nm

Table d.t.4.

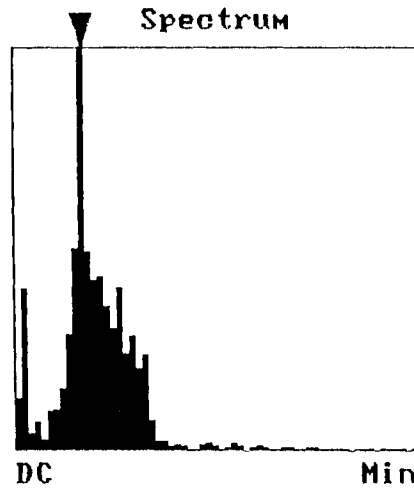
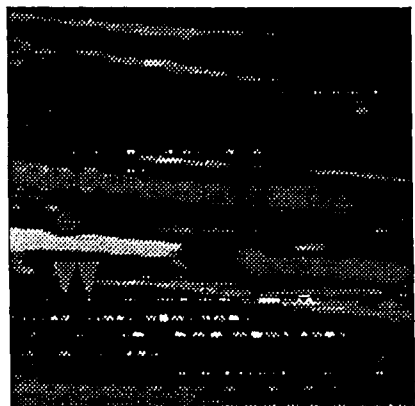
scan (size $3\mu\text{m}$)				gains		disturbance
number	rate	type	#samples	integral	proport.	
1.031	7	height	128	5	4	impulse from side
1.033	5	height	128	4	4	impulse on top
1.033	5	height	128	4	4	impulse on table
1.034	5	height	128	4	4	impulse on disk drum
1.035	5	height	128	4	4	impulse from side (size 10nm)
1.036	3	height	128	4	4	impulse from side, legs extended

Figure d.15. Scan #1.031

Section Analysis

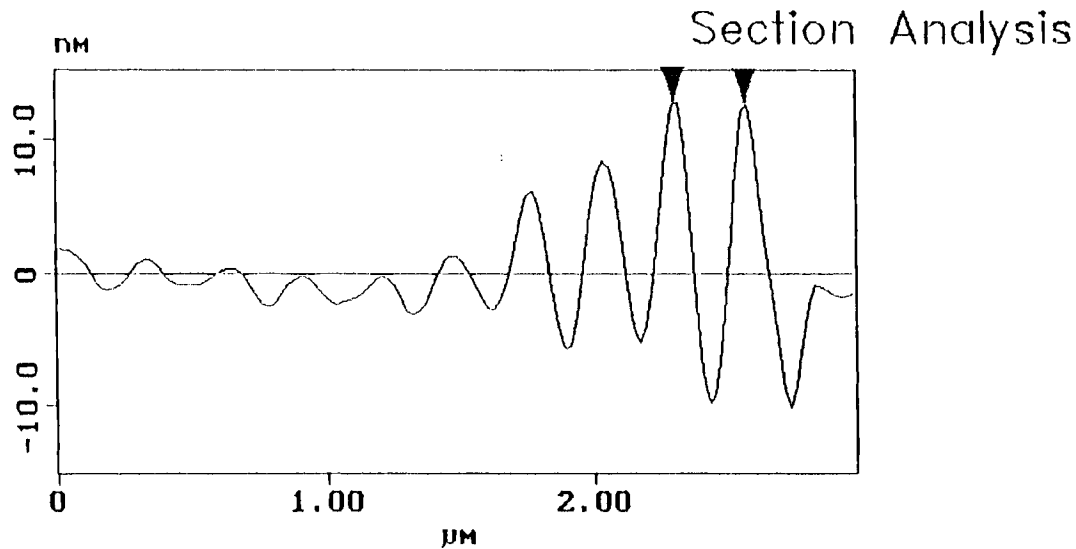


L	187.50 nm
RMS	5.834 nm
lc	276.89 nm
Ra(lc)	1.514 nm
Rmax	11.546 nm
Rz	11.546 nm
Rz Cnt	2

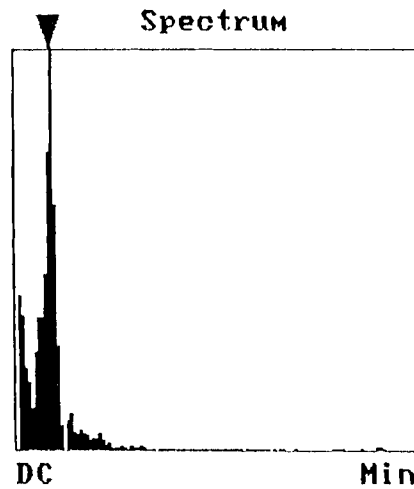


Horiz distance(L)	187.50 nm
Vert distance	12.259 nm
Angle	3.741 deg
Horiz distance	
Vert distance	
Angle	
Horiz distance	
Vert distance	
Angle	
Spectral period	276.89 nm
Spectral freq	146.95 Hz
Spectral amp	8.568 nm

Figure d.16. Scan #1.031

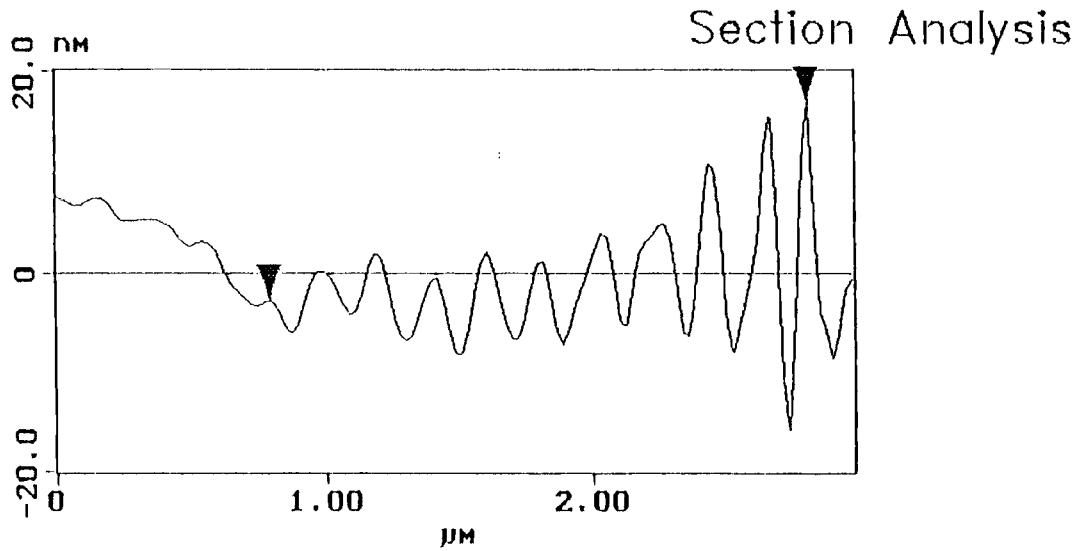


L	257.81 nm
RMS	8.377 nm
lc	270.60 nm
Ra(lc)	2.689 nm
Rmax	24.350 nm
Rz	24.350 nm
Rz Cnt	2

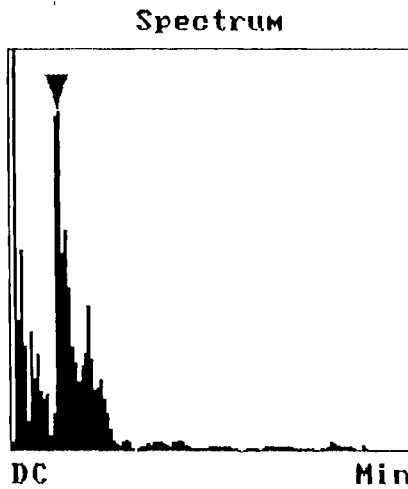


Horiz distance(L)	257.81 nm
Vert distance	0 nm
Angle	0 deg
Horiz distance	
Vert distance	
Angle	
Horiz distance	
Vert distance	
Angle	
Spectral period	270.60 nm
Spectral freq	150.37 Hz
Spectral amp	2.459 nm

Figure d.17. Scan #1.033

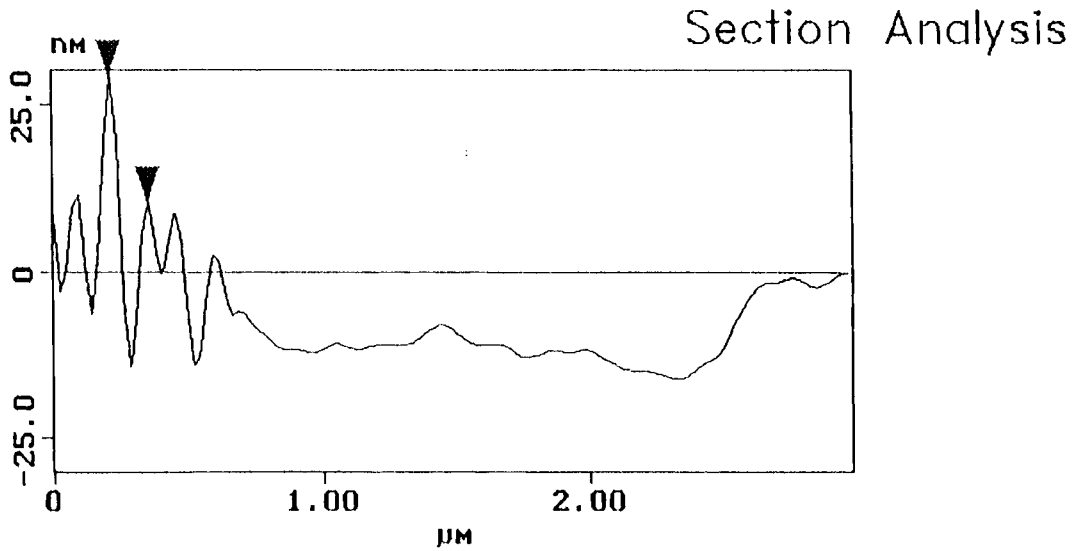


L	2.016 μm
RMS	5.509 nm
lc	198.44 nm
Ra(lc)	1.361 nm
Rmax	33.220 nm
Rz	18.559 nm
Rz Cnt	valid

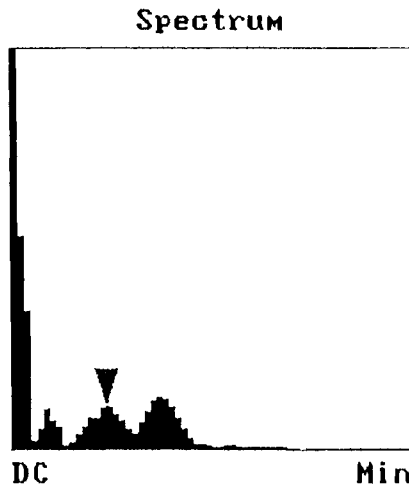


Horiz distance(L)	2.016 μm
Vert distance	20.087 nm
Angle	0.571 deg
Horiz distance	
Vert distance	
Angle	
Horiz distance	
Vert distance	
Angle	
Spectral period	198.44 nm
Spectral freq	150.65 Hz
Spectral amp	2.125 nm

Figure d.18. Scan #1.033



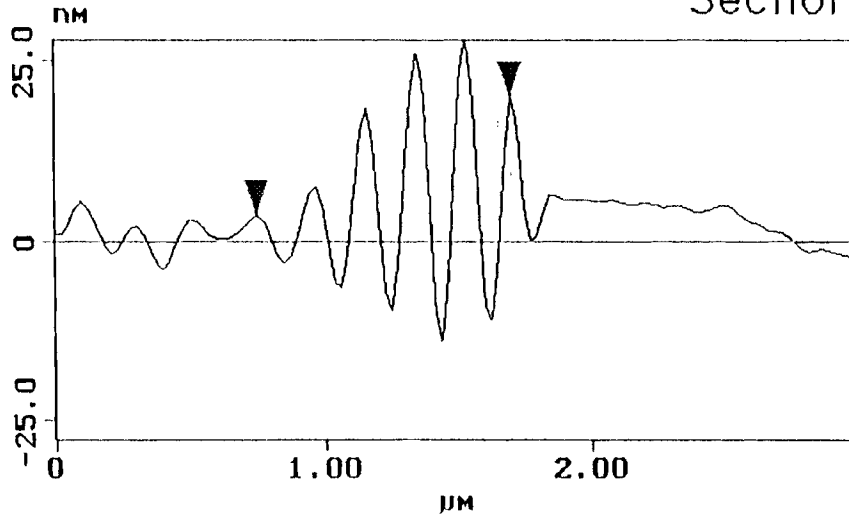
L	140.63 nm
RMS	14.382 nm
lc	198.44 nm
Ra(lc)	4.490 nm
Rmax	36.265 nm
Rz	36.265 nm
Rz Cnt	2



Horiz distance(L)	140.63 nm
Vert distance	19.127 nm
Angle	7.745 deg
Horiz distance	
Vert distance	
Angle	
Horiz distance	
Vert distance	
Angle	
Spectral period	198.44 nm
Spectral freq	150.65 Hz
Spectral amp	1.102 nm

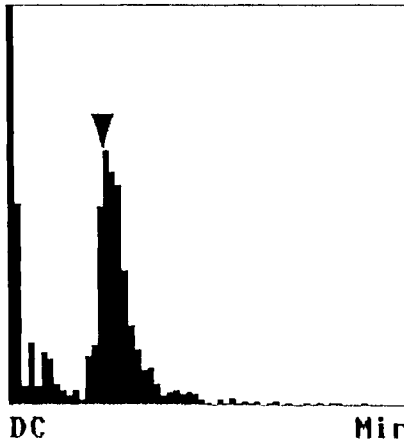
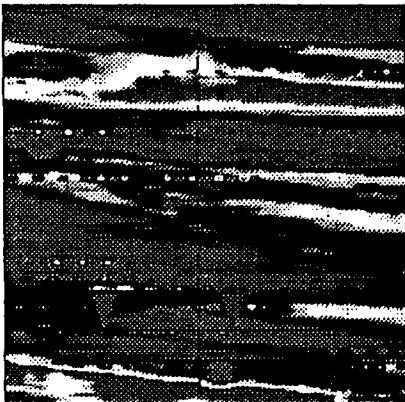
Figure d.19. Scan #1.034

Section Analysis



L	937.50 nm
RMS	11.010 nm
lc	198.44 nm
Ra(lc)	3.183 nm
Rmax	41.536 nm
Rz	27.782 nm
Rz Cnt	valid

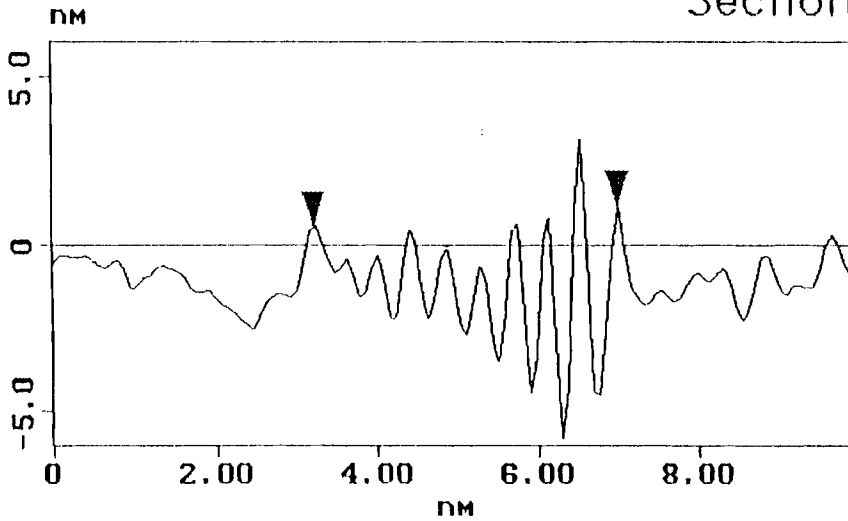
Spectrum



Horiz distance(L)	937.50 nm
Vert distance	16.395 nm
Angle	1.002 deg
Horiz distance	
Vert distance	
Angle	
Horiz distance	
Vert distance	
Angle	
Spectral period	198.44 nm
Spectral freq	150.65 Hz
Spectral amp	3.059 nm

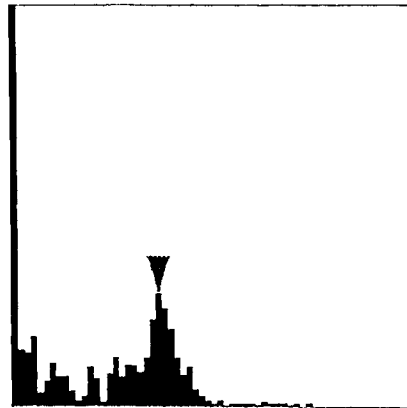
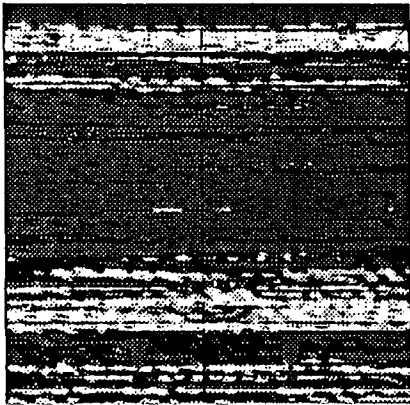
Figure d.20. Scan #1.035

Section Analysis



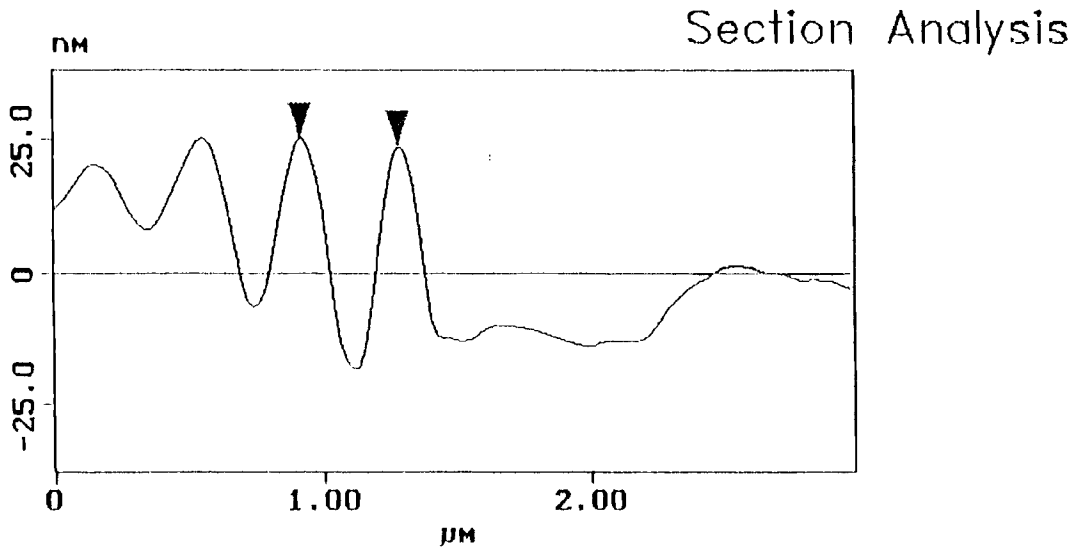
L	3.750 nm
RMS	1.742 nm
lc	0.422 nm
Ra(lc)	0.416 nm
Rmax	8.930 nm
Rz	5.427 nm
Rz Cnt	valid

Spectrum

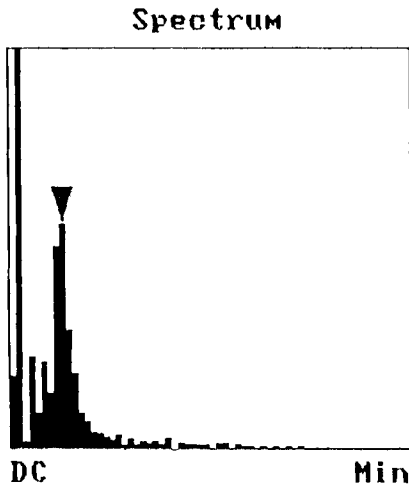
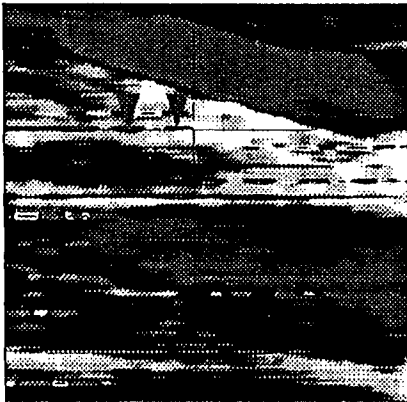


Horiz distance(L)	3.750 nm
Vert distance	0.591 nm
Angle	8.956 deg
Horiz distance	
Vert distance	
Angle	
Horiz distance	
Vert distance	
Angle	
Spectral period	0.422 nm
Spectral freq	236.02 Hz
Spectral amp	0.456 nm

Figure d.21. Scan #1.036



L	351.56 nm
RMS	15.978 nm
lc	350.18 nm
Ra(lc)	5.150 nm
Rmax	45.629 nm
Rz	45.417 nm
Rz Cnt	2

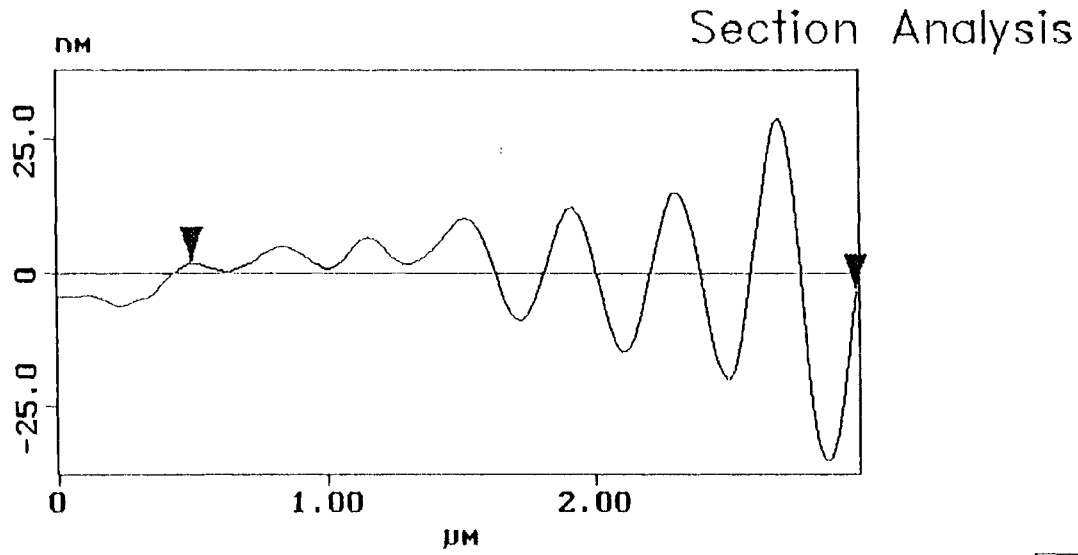


Horiz distance(L)	351.56 nm
Vert distance	1.475 nm
Angle	0.240 deg
Horiz distance	
Vert distance	
Angle	
Horiz distance	
Vert distance	
Angle	
Spectral period	350.18 nm
Spectral freq	85.369 Hz
Spectral amp	5.185 nm

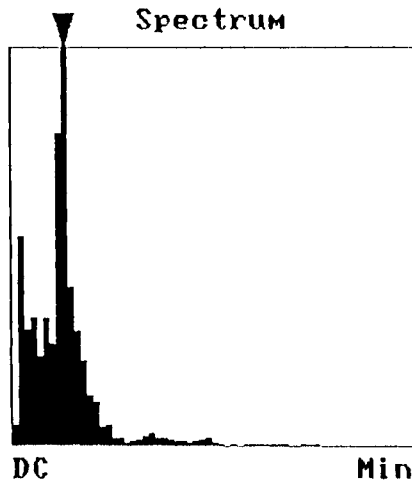
Table d.t.5.

scan (size $3\mu\text{m}$)		gains				disturbance
number	rate	type	#samples	integral	proport.	
2.010	5	height	128	5	7	impulse on side, legs extended
2.012	3	height	128	10	14	impulse on side, legs extended
2.0117	5	height	128	5	7	impulse on top, legs retracted
2.017	5	height	128	5	7	impulse on side, legs retracted

Figure d.22. Scan #1.036

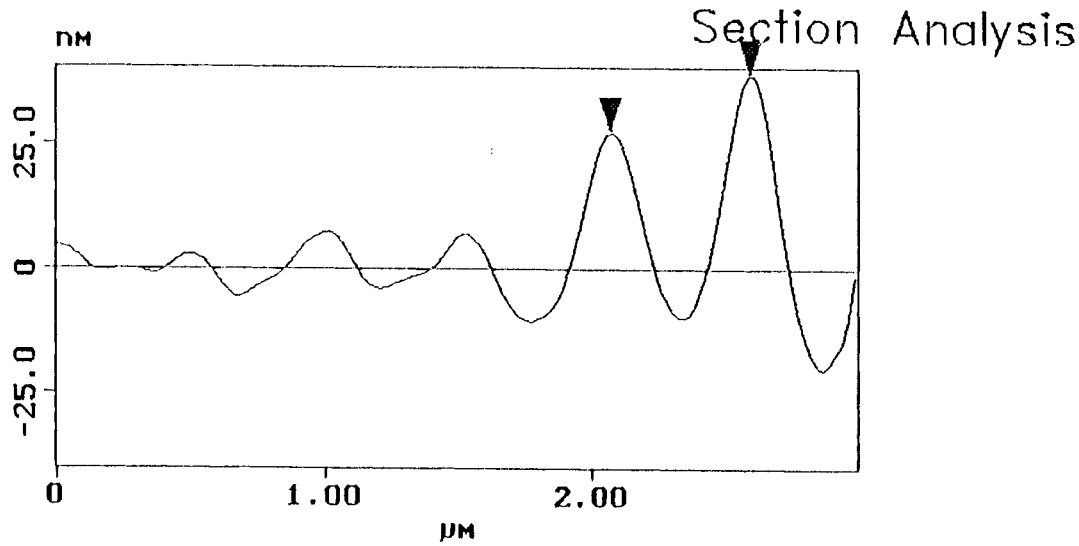


L	2.461 μm
RMS	11.728 nm
lc	350.18 nm
Ra(lc)	2.693 nm
Rmax	63.325 nm
Rz	29.979 nm
Rz Cnt	valid

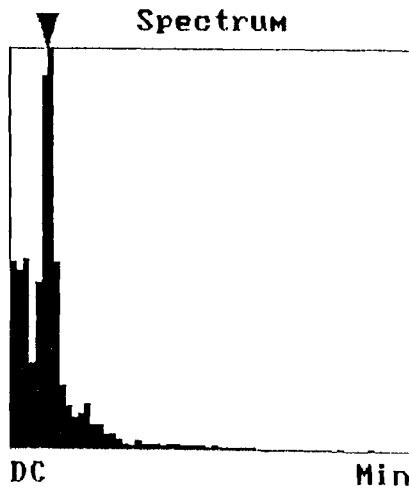
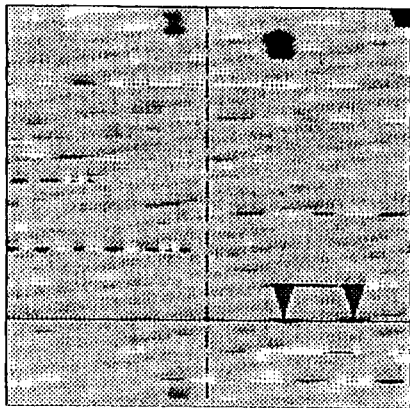


Horiz distance(L)	2.461 μm
Vert distance	5.019 nm
Angle	0.117 deg
Horiz distance	
Vert distance	
Angle	
Horiz distance	
Vert distance	
Angle	
Spectral period	350.18 nm
Spectral freq	85.369 Hz
Spectral amp	6.634 nm

Figure d.23. Scan #2.010

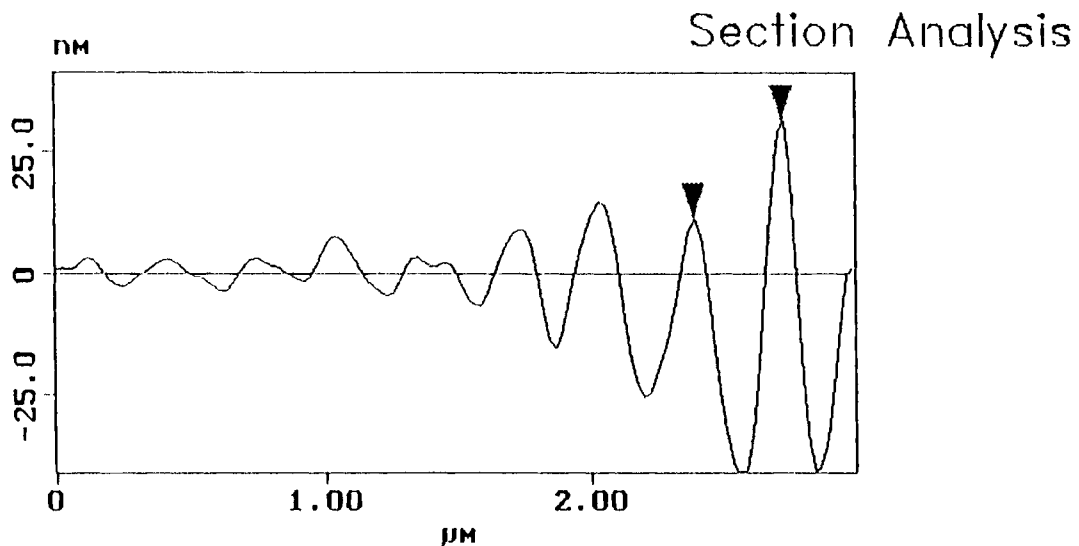


L	515.63 nm
RMS	16.221 nm
lc	496.09 nm
Ra(lc)	5.056 nm
Rmax	43.829 nm
Rz	43.829 nm
Rz Cnt	2

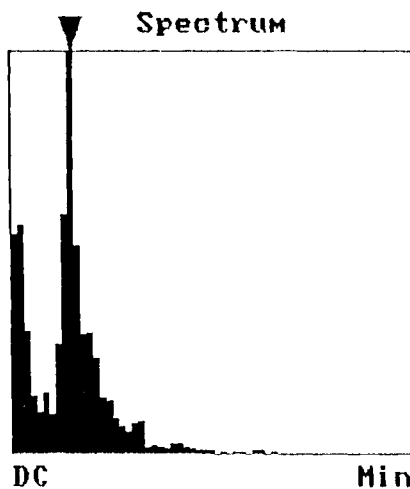
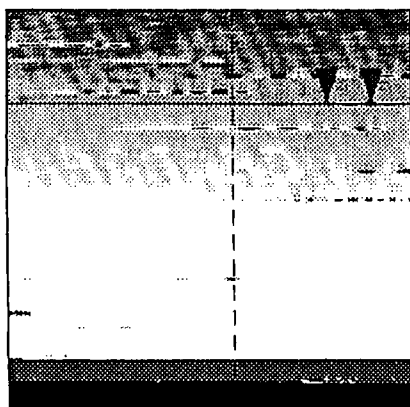


Horiz distance(L)	515.63 nm
Vert distance	11.742 nm
Angle	1.304 deg
Horiz distance	
Vert distance	
Angle	
Horiz distance	
Vert distance	
Angle	
Spectral period	496.09 nm
Spectral freq	60.260 Hz
Spectral amp	6.859 nm

Figure d.24. Scan #2.012

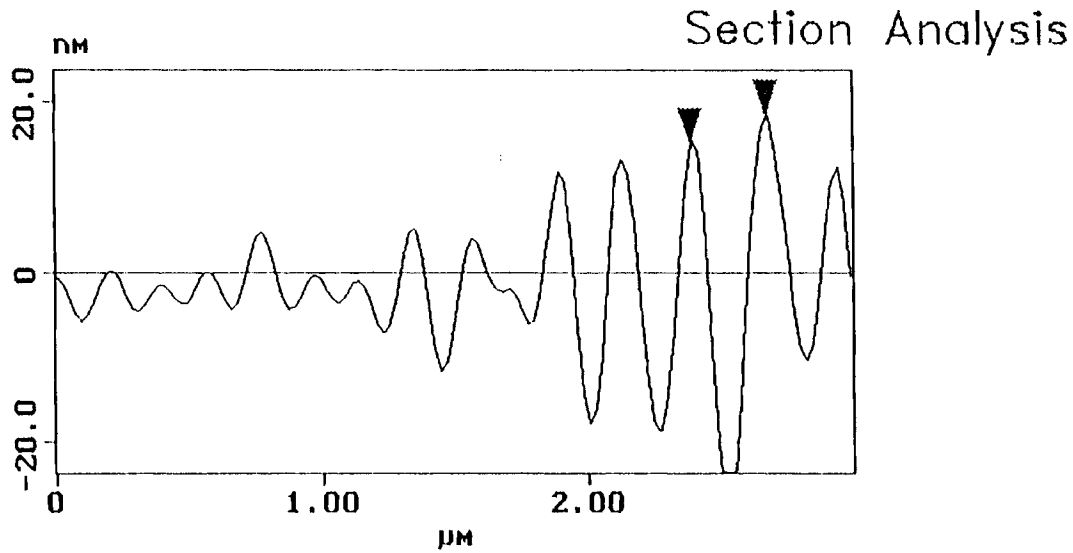


L	328.13 nm
RMS	24.644 nm
lc	305.29 nm
Ra(lc)	7.340 nm
Rmax	64.561 nm
Rz	64.561 nm
Rz Cnt	2

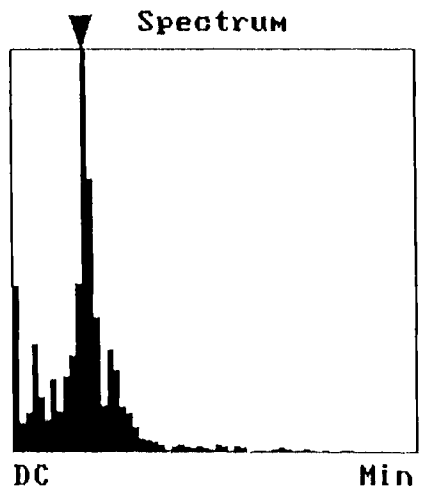
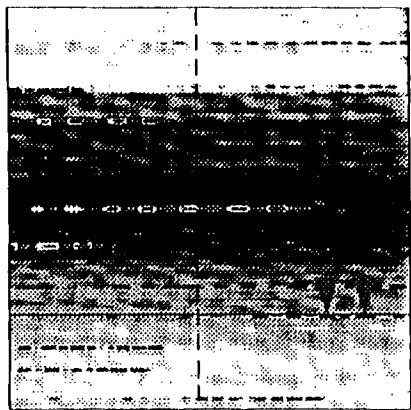


Horiz distance(L)	328.13 nm
Vert distance	20.677 nm
Angle	3.606 deg
Horiz distance	
Vert distance	
Angle	
Horiz distance	
Vert distance	
Angle	
Spectral period	305.29 nm
Spectral freq	59.237 Hz
Spectral amp	8.290 nm

Figure d.25. Scan #2.017

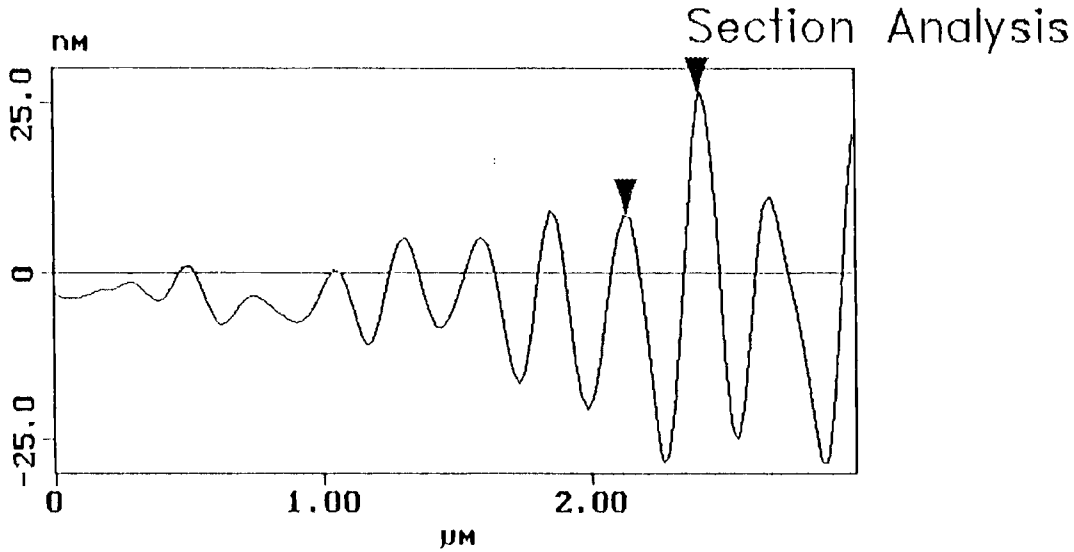


L	281.25 nm
RMS	17.107 nm
lc	264.58 nm
Ra(lc)	5.310 nm
Rmax	49.141 nm
Rz	49.141 nm
Rz Cnt	2

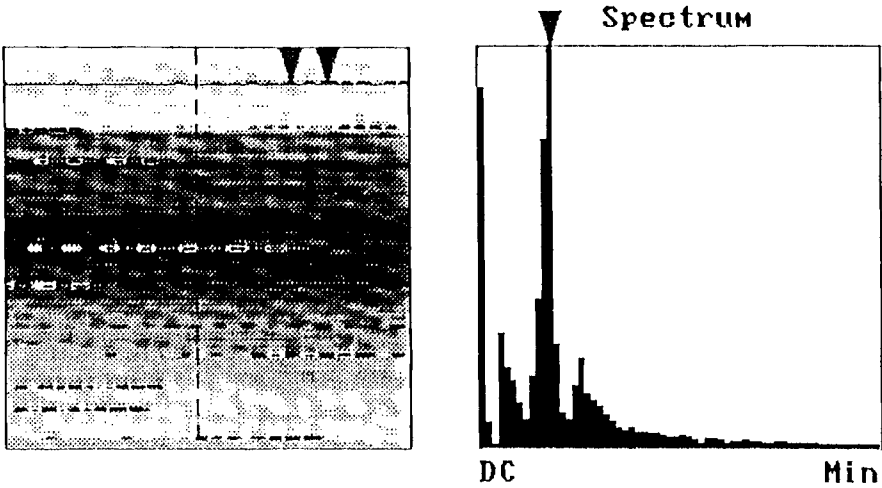


Horiz distance(L)	281.25 nm
Vert distance	3.027 nm
Angle	0.617 deg
Horiz distance	
Vert distance	
Angle	
Horiz distance	
Vert distance	
Angle	
Spectral period	264.58 nm
Spectral freq	112.99 Hz
Spectral amp	5.449 nm

Figure d.26. Scan #2.017



L	257.81 nm
RMS	17.545 nm
lc	253.32 nm
Ra(lc)	5.115 nm
Rmax	46.982 nm
Rz	46.756 nm
Rz Cnt	2



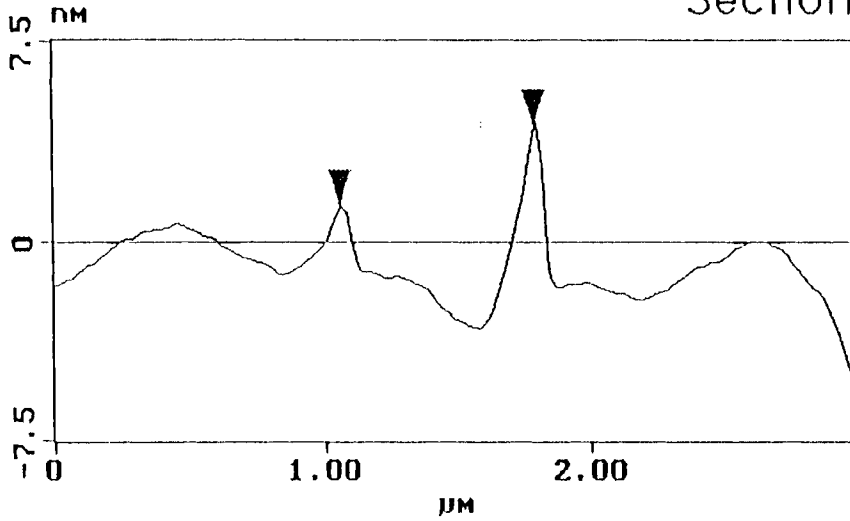
Horiz distance(L)	257.81 nm
Vert distance	19.053 nm
Angle	4.227 deg
Horiz distance	
Vert distance	
Angle	
Horiz distance	
Vert distance	
Angle	
Spectral period	253.32 nm
Spectral freq	118.01 Hz
Spectral amp	6.505 nm

Table d.t.6.

scan (size $3\mu\text{m}$)		gains				disturbance
number	rate	type	#samples	integral	proport.	
2.006	5	height	128	2	3	impulse on side
2.008	3	height	128	2	3	impulse on top

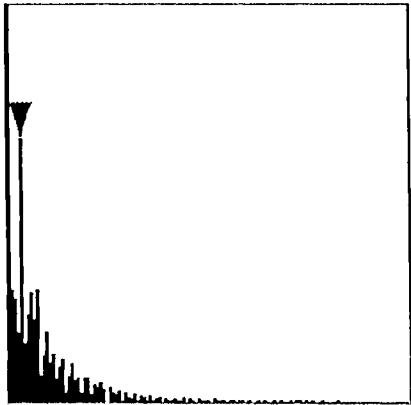
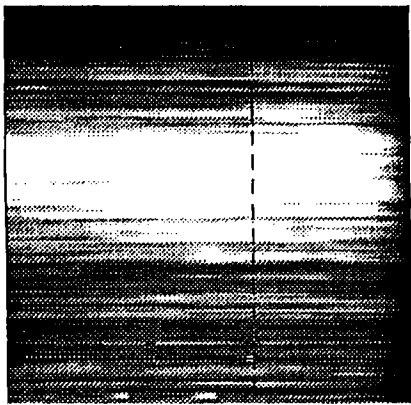
Figure d.27. Scan #2.006

Section Analysis



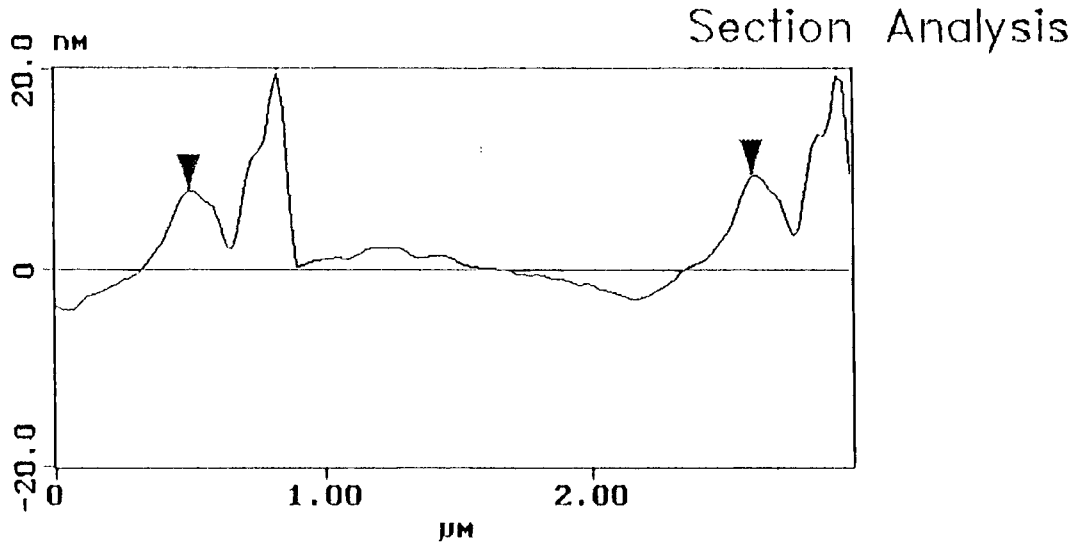
L	726.56 nm
RMS	1.864 nm
lc	661.46 nm
Ra(lc)	0.476 nm
Rmax	7.626 nm
Rz	7.494 nm
Rz Cnt	2

Spectrum

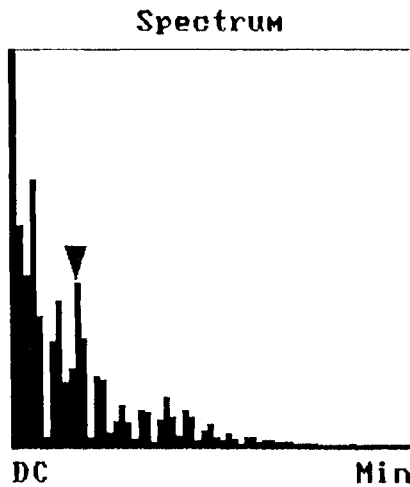
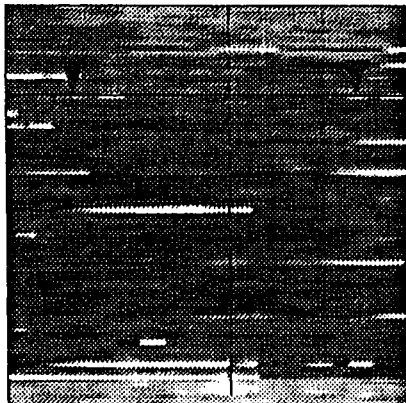


Horiz distance(L)	726.56 nm
Vert distance	3.176 nm
Angle	0.250 deg
Horiz distance	
Vert distance	
Angle	
Horiz distance	
Vert distance	
Angle	
Spectral period	661.46 nm
Spectral freq	45.195 Hz
Spectral amp	0.840 nm

Figure d.28. Scan #2.008



L	2.109 μm
RMS	4.466 nm
lc	290.40 nm
Ra(lc)	0.484 nm
Rmax	18.643 nm
Rz	16.227 nm
Rz Cnt	4



Horiz distance(L)	2.109 μm
Vert distance	1.624 nm
Angle	0.044 deg
Horiz distance	
Vert distance	
Angle	
Horiz distance	
Vert distance	
Angle	
Spectral period	290.40 nm
Spectral freq	61.516 Hz
Spectral amp	1.601 nm

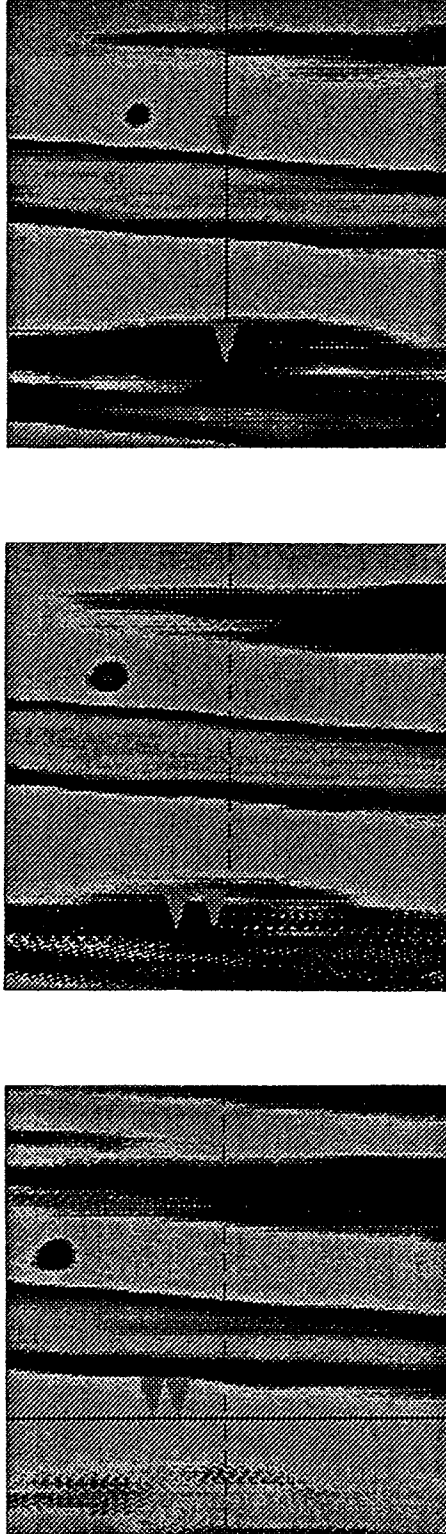


Figure d.29. Thermal drifts

VITA 1

Thomas G. Marelli

Candidate for the Degree of

Master of Science

Thesis: ON THE VIBRATORY RESPONSE OF THE STANDALONE ATOMIC
FORCE MICROSCOPE

Major Field: Mechanical Engineering

Biographical:

Personal Data: Born in Milano, Italy, January 8, 1963, the son of artists Angelo and Virginia Marelli.

Education: Salutorian with special diploma and physics award from St. John's Military School, Salina, Kansas, in May 1981; Bachelor of Science in Physics and Bachelor of Arts in Classics from the University of Oklahoma in May 1991; completed requirements for the Master of Science Degree at Oklahoma State University in May 1995.

Professional Experience: CAD Draftsman, Physical Plant Administration, Oklahoma State University September 1994, to April 1995.
Italian Instructor, Department of Modern Languages, the University of Oklahoma, Spring semester of 1992.
Research Assistant Department of Physics and Astronomy, the University of Oklahoma, Summer 1990.